MODAL ANALYSIS OF VERTICAL-AXIS DARRIEUS WIND TURBINE BLADE WITH A TROPOSKEIN SHAPE

By

Amr Fawzy Abdel hakeem Saleh

A THESIS

Submitted to
Michigan State University
in partial fulfillment of the requirements
for the degree of

Mechanical Engineering - Master of Science

2017

ABSTRACT

MODAL ANALYSIS OF VERTICAL-AXIS DARRIEUS WIND TURBINE BLADE WITH A TOPOSKEIN SHAPE

By

Amr Fawzy Abdel hakeem Saleh

Darrieus wind turbines with troposkein shaped blades are an important type of vertical axis wind turbines. When designing these turbines it is important to consider how vibrations may affect blade failure. In order to avoid resonance, the blade natural frequencies need to be determined. The goal of this research is to determine the blade free vibration mode shapes and modal frequencies, neglecting the variation of the upstream wind speed for simplicity. The blade modal vibration is studied numerically using ANSYS software, and analytically using thin-beam theory and an assumed modes method. Firstly, the analysis is performed on a 17 m diameter Sandia simplified troposkein shaped blade with a NACA 0015 airfoil. The first ten modes and the corresponding natural frequencies were calculated using ANSYS. The analysis was done for stationary and spinning blade at 54 rpm. The spin case compared very well to previous Sandia results. The same analysis was then applied to an ideal troposkein shaped blade, and a slightly modified cross section. Results show consistency across the blade shapes. The Sandia blade shape was studied analytically using thin-beam theory and an assumed modes method. Kinetic and potential energies were derived. Mass and stiffness matrices are formulated for the discretized model, to which modal analysis is applied. The natural frequencies were calculated analytically for same simplified Sandia blade shape used for finite element model under stationary condition. The results of the two methods were compared for consistency.

I would like to dedicate this work to my mother and my father's soul, and my lovely wife

ACKNOWLEDGMENTS

I would like to thank my advisor and my master Professor Brian Feeny for his endless technical and mental support and sharing his wisdom generously to influence me to go further. Without his dedication this research would have never existed.

TABLE OF CONTENTS

LIST OF TABLES

LIST OF FIGURES

1 Chapter 1: Introduction and literature review

1.1 Background

The development of renewable energy represents an obvious need especially when we see based on modern studies that fossil fuel sources like oil and gas reserve will be depleted in near future. Renewable energy can be solar energy, wind energy, geothermal energy,etc. Among the renewable energy alternatives, wind energy introduces itself as one of the most prominent sources of renewable energy. Wind turbines are the most popular machines that can convert wind power into mechanical power. Wind turbines convert the wind power into electricity via rotation in the generator. Now, after large technological improvements, we are able to develop wind turbines to be more feasible, reliable, and dependable source of energy especially for electricity. Indeed, a significant share of electricity for several countries comes from wind turbines. Figure 1.1 indicates the growth of global wind power production over years from 1996 to 2015 [1].

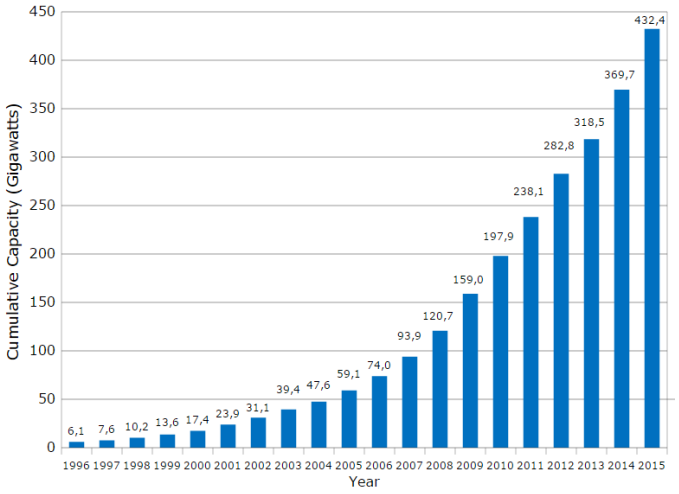

Figure 1.1 Global wind power cumulative capacity [1]

1.2 Types of wind converters

Wind energy converters can be classified firstly in accordance with their constructional design (rotor axis orientation) and, secondly, according to their ways of extracting the energy from wind (lift or drag type) [2].

1.2.1 Constructional design (rotor axis orientation) based classification

1.2.1.1 Vertical axis wind turbines (VAWTs):

As shown in Figure.1.2. The axis of rotation of this type is perpendicular to the wind direction [2]. In this type the generator is on the ground which makes it more accessible and no yaw system required.

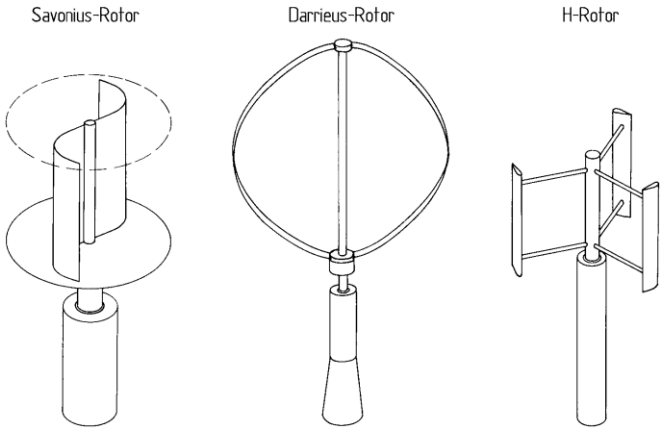

Figure 1.2 Schematic of vertical axis wind turbine [2]

The constant blade profile and cross sectional shape of an H-rotor type VAWT along the blade length is one of its advantages because it makes every blade section be subjected to the same wind speed. As a result blade twisting not required. Troposkein-shaped turbines also tend to have constant cross-sectional shapes.

The constant blade shape makes its design and manufacturing easier and the total production cost lower.

1.2.1.2 Horizontal axis wind turbines (HAWTs):

As shown in figure 1.3 [2] the axis of rotation of this type must be oriented parallel to the wind in order to capture the wind power. HAWTs are considered to be the most efficient turbines. The disadvantages of this type include:

a. Operation at high starting wind velocity.
b. Low starting torque.
c. Yaw mechanism required to turn the rotor toward the wind.
d. Power loss when the rotors are tracking the wind directions.
e. High center of gravity.

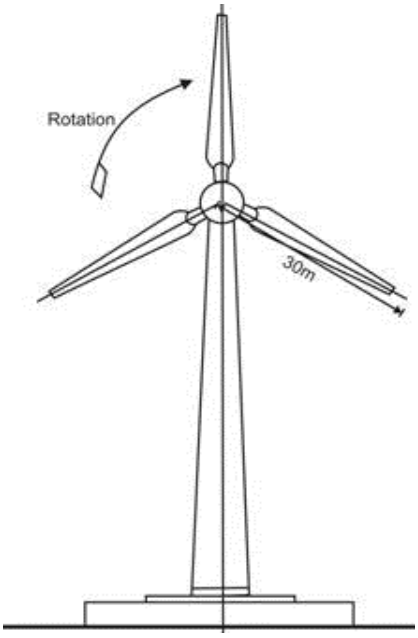

Figure 1.3 Schematic of horizontal wind turbine [2]

1.2.2 Classification based on ways of extracting the energy from wind (lift or drag type)

The rotor's aerodynamics is classified based on whether the wind energy converter captures its power from the aerodynamic drag of the air flow over the rotor surfaces, or whether it captures its power from the aerodynamic lift generated from the air flow against the airfoil surfaces [2]. Based on that, there are so-called ***drag-type rotors*** and ***lift- type rotors***.

1.2.2.1.1 The drag type

This turbine takes less energy from the wind but provides a higher torque and is suitable for mechanical applications as water pumping [2]. The most representative model of a drag-type VAWT as shown in Figure 1.4 [3] is the Savonius.

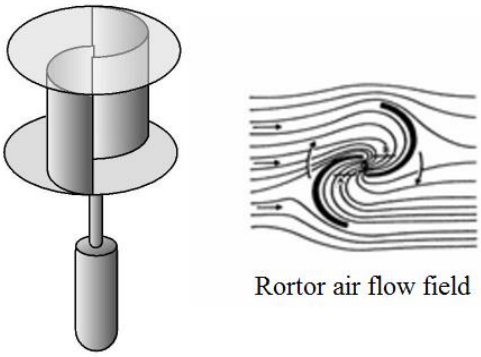

Figure 1.4 Schematic of Savonius wind turbine [3]

1.2.2.2 The lift type

This turbine generates power mainly by the generated lift force on the blade cross section. It can move quicker than the free wind speed. The most important application of this kind

is electricity generation [2]. The most representative model of a lift-type VAWT as shown in Figure 1.4 [4] is the Darrieus wind turbine.

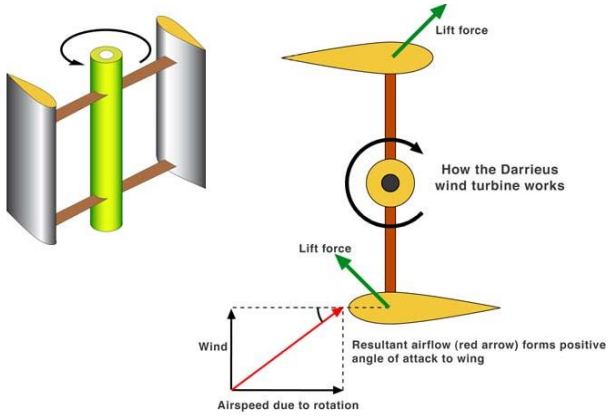

Figure 1.5 Schematic of Darrieus wind turbine [4]

In 1931 the U.S. Patent Office patented Darrieus wind turbine in the name of G.J.M. Darrieus [5]. The Darrieus patent states that *"each blade should have a streamline outline curved in the form of skipping rope."* [5] This means, the shape of the Darrieus rotor blades can be approximated to the shape of a perfectly flexible cable, of uniform density and cross section, anchored from two fixed points and rotating about its long axis; under the effect of centrifugal forces such a shape minimizes inherent bending stresses. This blade shape is called troposkien (from the Greek roots: *τροτς*, turning and *σχοlvlου*, rope). A pure troposkien shape (gravity neglected) does not depend on angular velocity [6]. The equation that defines a troposkein blade profile was developed by Sandia in April 1974 [7]. The analysis considered a perfectly flexible cable rotating about a fixed axis at a constant angular velocity without gravity as shown in figure 1.6. *The Darrieus wind turbine with a troposkien shaped blades has advantage of working under the effect of high centrifugal forces without failure.*

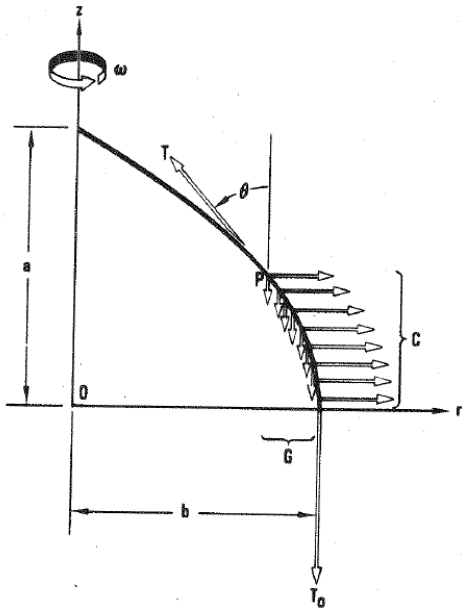

Figure 1.6 Schematic of a perfectly flexible cable rotating about a vertical axis [7]

1.3 Literature survey of the structural vibration analysis of vertical axis troposkein shaped wind turbine blade

The performance of a Darrieus wind-turbine was studied firstly by R.S. Rangi and P. South using wind tunnel measurements in the National Research Council of Canada in March 1971 [8]. In February 1974, R.S. Rangi and P. South and their team investigated Darrieus wind parameters including spoilers and aero-brakes effect on turbine performance and reliability, in addition to the effect of efficiency related parameters like the number of blades and the rotor's solidity. Compared to Sandia's simplified troposkein shape, the engineers at the National Research Council of Canada (NRC) in the early 1970's, independently developed catenary shape as an approximation to the troposkein curved

blade [9]. In December 1979 a NASA team developed second degree nonlinear aero-elastic partial differential equations of motion for a slender, flexible, non-uniform, Darrieus vertical axis wind turbine blade using Hamilton's principle. The analysis of NASA team considered a blade undergoing combined flat-wise bending, edgewise bending, torsion, and extension. Flatwise and edgewise are defined as follows. The airfoil cross section has a major (chord-length) and minor axis. Bending about the major axis is referred to as "flat wise", and bending about the minor axis is called "edge-wise." Extension refers to axial deformation, and torsion occurs about the elastic axis [can cite an elasticity book regarding elastic axis].The blade aero-dynamic loading was developed using *strip theory based on a quasi-steady approximation of two-dimensional incompressible unsteady airfoil theory* [10]. The derivation of the equations of motion was done based on the geometric nonlinear theory of elasticity in which the elongations and shears (and hence strains) are negligible compared to unity. In this research work The NASA model was used to derive equations of the blade strain energy and kinetic energy. These equations are suitable to study the blade free vibration and the blade dynamic response [10].

In June 1979, Sandia introduced a modal analysis for a 17-m diameter simplified troposkein shape rotating at 54 rpm constant angular velocity using ANSYS finite element software. This simplified troposkein blade consists of two straight increments at both ends and circular part in the middle (described in details later) with a NASA 0015 airfoil cross section. The first eight natural frequencies were calculated and the corresponding mode shapes were produced [11].

Another wind tunnel performance analysis for the Darrieus wind turbine with NACA 0012 Blades was performed in Sandia by Bennie F. Blackwell, Robert E. Sheldahl, and Louis V.

Feltz [12], where several configurations of Darrieus wind turbine blade with NASA 0012 airfoil cross section and 2- meters diameter were tested in a low-speed wind tunnel to measure the output torque, rotational speed as a function of rotor solidity, Reynolds number, and the free stream wind velocity. A significant step in the development of larger and more efficient commercial Darrieus VAWT's was the installation and operation of 34-m Sandia-DOE VAWT in 1987, rated at 625 kW. The Sandia 34-m turbine (Fig. 1.7) was the first curved-blade Darrieus turbine rotor originally designed to incorporate step-tapered blades using varying blade-section airfoils and a blade airfoil section specifically designed for VAWTs [6].

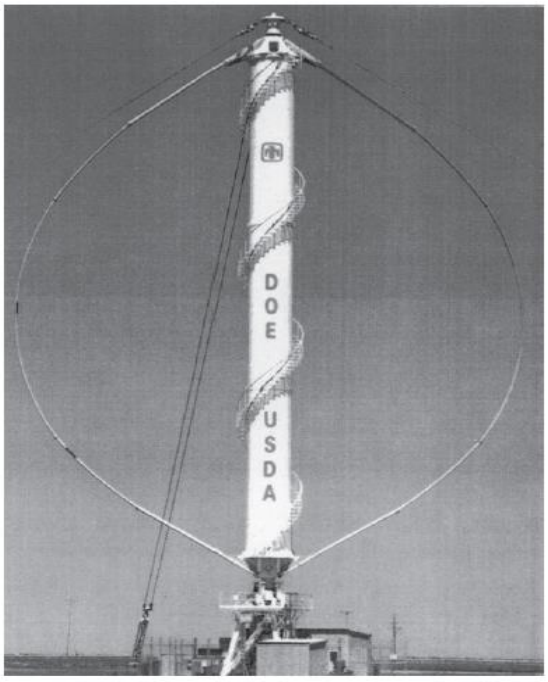

Figure 1.7 Darrieus vertical-axis wind turbine (DOE/Sandia 34-m) [6]

In 2014 a structural dynamic design tool developed by Sandia for large scale VAWTs for studying the effect of geometry configuration, blade material, and number of blades on the aeroelastic stability of VAWTs. This tool can describe quantitatively the aeroelastic

instabilities in VAWT design [13]. This is part of a recent strong research effort led by Sandia to study VAWTs, motivated by the prospect of off-shore applications. Their work has addressed the modeling of aeroelastic loading and the vibration responses, ultimately for guiding the design and manufacture of VAWT systems, and has involved the development of finite-element-based OWENS simulation toolkit, modal analysis of blade-tower systems, potential for resonances, and field tests on the Sandia 34-m VAWT test bed [14-16]. Further interest in structural modeling of VAWTs is represented by a series of presentations at a recent conference dedicated to off-shore VAWTs [17].

1.4 Motivation

The following facts indicate why we need deep and active research on Darrieus vertical axis wind turbines:

1. Limited knowledge and experience about Darrieus VAWTs
2. Large scaled HAWTs suffer failures due cyclic gravitational and aerodynamic loadings. Darrieus VAWTs offers a good solution for this problem because of the blade shape which minimizes inherent bending stresses and rotor vertical position which minimizes the gravitational effect, so by developing a large scale Darrieus VAWTs and improving VAWT dynamic behavior can provide an alternative to problematic HAWTs without losing advantage of high energy production.
3. Further investigation and more study of VAWTs dynamics and vibration can increase its life and as a result save a lot of money
4. All research in the field of troposkein shape blade dynamics was basically for the simplified and approximated shape. Now with the help of high performance computers

and advanced calculation techniques, it is time to investigate the ideal troposkein blade dynamics and how we can optimize this shape to get efficient blade performance.

1.5 Objective

This research aims to formulate a robust model for a troposkein shaped VAWT blade for studying the blade vibration and its mode shapes and natural frequencies, taking into account the blade loading and geometric complexities, which help us determine the safe margins for the blade operating loads and angular velocities.

1.6 Thesis outline

This research is presented in the next two chapters:

Chapter 2 focuses on the finite-element analysis of the blade vibration, while chapter 3 sketches an analytical beam-based model for vibration studies.

More specifically, chapter 2 consists of the following:

1. Modal analysis is done using ANSYS workbench software for Darrieus wind turbine blade with NASA 0015 airfoil for both simplified and ideal troposkein shapes.
2. Model validation is performed by comparing the mode shapes and natural frequencies of the first eight modes to those of the Sandia model [11].
3. The effect of spinning on the model vibration is then examined

   Chapter 3 consists of the following:
4. Kinetic and potential energies equations are derived and mass and stiffness matrices are formulated to be used in Lagrange's equation to calculate the natural frequencies and mode shapes analytically.

2 Chapter 2: Finite element model for calculating mode shapes and modal frequencies of troposkein shaped vertical axis wind turbine blades

2.1 Introduction

The wind turbine structure will oscillate due to cyclic aerodynamic loads during operation. Because the turbine is a continuous system with many degrees of freedom it has many different modes of oscillation and many corresponding natural frequencies. The most critical component of the wind turbine is the blades. In this chapter a finite element modal analysis has been done using ANSYS WORKBENCH finite element software.

In the first part of this chapter a model for a 17-m diameter straight-circular-straight shape suggested by Sandia as an approximation to the ideal troposkein shape has been built using inventor software. This wind turbine blade model has a 17-m diameter with 25.15 m height and 30.48 m total blade length. The blade cross section is a NASA-0015 airfoil with chord length 0.61 m, airfoil thickness of 0.091 m and wall thickness 6.35 mm except for the reinforced leading edge which has a wall thickness of 8.89 mm.

The blade cross section has four uniform internal stiffeners with the same thickness of the wall. The stiffeners are strategically located to provide enough structural rigidity.

A free vibration modal analysis for this model has been performed using ANSYS WORKBENCH under constant rotational velocity of 54 rpm with blade ends clamped. To validate this model the results of the analysis compared to the results of Sandia report [11].

After validating our model, the vibrations of a stationary blade are studied. A stationary blade condition is useful as a benchmark for stationary laboratory experiments or comparison between models. It also helps to understand the effect of spin.

In the second part of this chapter a model for the ideal troposkein shape has been built and analyzed to get the mode shapes and modal frequencies of the ideal troposkein shape and to compare the approximated blade shape of the straight-circular-straight segmented beam to the ideal shape.

2.2 3-D model for 17m diameter blade of straight-circular-straight shape

2.2.1 Blade cross section

The blade airfoil is based on NASA's four digit airfoils equation [18] as follows

$$y_t = \frac{t}{0.2}\left(0.2969\sqrt{\frac{x}{c}} - 0.126\frac{x}{c} - 0.3516\left(\frac{x}{c}\right)^2 + 0.2843\left(\frac{x}{c}\right)^3 - 0.1015\left(\frac{x}{c}\right)^4\right) \qquad (2.1)$$

where

c is the chord length

t is the maximum airfoil thickness which equals 0.15c

x is the coordinates of the airfoil along the chord or the major axis

y_t is the coordinates of the airfoil along the minor axis

For a NASA 0015 airfoil with 0.61 m cord length, the blade cross section shape can be calculated using equation (2.1) and its coordinates as given in table A.1 in appendix A.

Plotting y versus x from table A.1 gives the airfoil shape as in figure 2.1

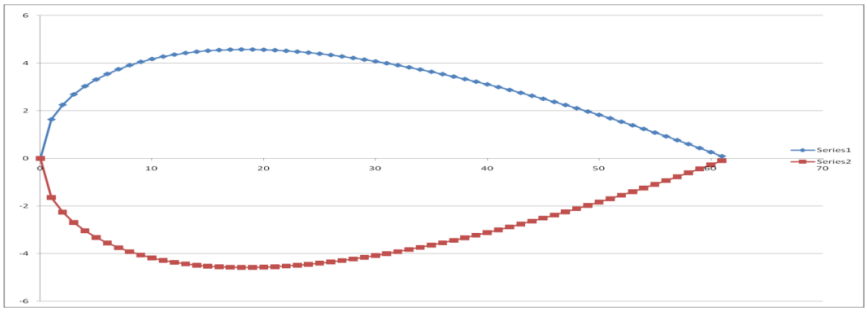

Figure 2.1 plot of airfoil points

Taking points of airfoil from table.1in the appendix and generating the shape of the outer and inner airfoils by Inventor software using the offset feature, then a four stiffening spars was generated by Inventor with 6.5 mm thickness each and strategically located to provide proper structural rigidity [11]. The final shape of the airfoil is shown in figure 2.2

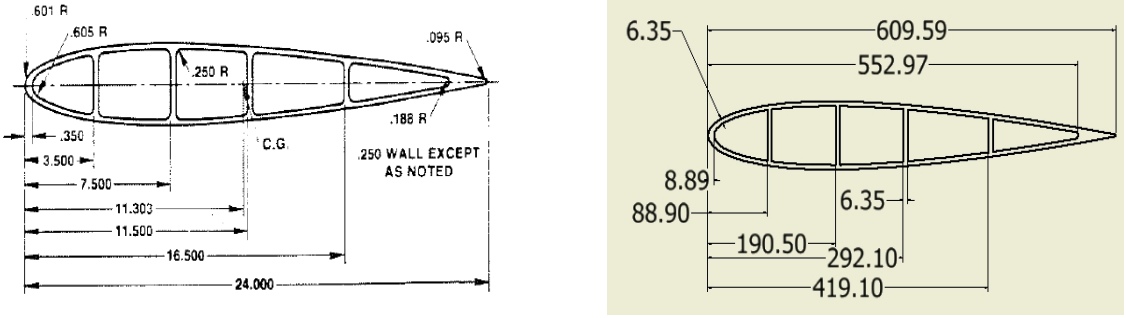

(a) (b)

Figure 2.2 NASA 0015 blade cross section of 17 m diameter Sandia blade. (a) The original Sandia one. (b) The one rebuilt for this work

2.2.2 Blade profile

The Sandia blade consists of three segments: one circular at the middle with radius 10.43 m and 16.754 m length and two straight segments of 6.858 m length each as indicated in figure 2.3.

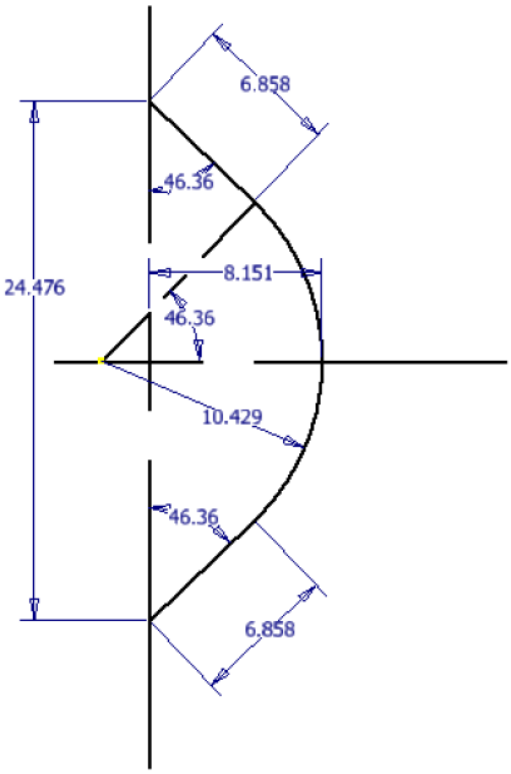

Figure 2.3 17 m diameter Sandia blade profile (all dimensions in m)

2.3 FEM model for 17m diameter blade of straight-circular-straight shape spins with 54 rpm constant rotational velocity

A modal analysis for the 17 m diameter Sandia blade has been done using ANSYS workbench by meshing the blade structure using the SOLID 187 element. The SOLID 187 is a ten nodes higher order 3-D element, which makes it well suited to model irregular meshes. A SOLID 187 element has three degrees of freedom at each node (translations in the nodal x, y, and z directions) [19]. The blade is clamped at both ends except for rotation about the y-axis as shown in figure 2.4 where the blade assumed to be rotating at constant rotational velocity of 54 rpm.

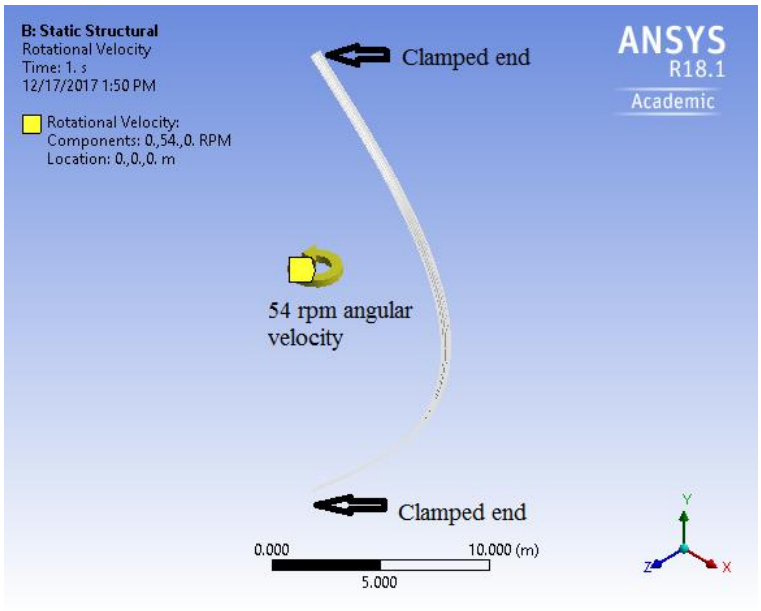

Figure 2.4 Sandia simplified blade shape clamped at both ends and allowed to rotate

Figure 2.5 indicates the mesh pattern generated by ANSYS. By magnifying a part of this mesh we can note the elements shapes. For this analysis of 17 m diameter simplified Sandia blade the element size refined several times starting from automatic mesh and going finer to see the effect of mesh refinement on the results. After refining the mesh in limits of ANSYS academic version available for our lab, we found that there is no significant difference in the results of different meshing cases. The modal results of simplified Sandia blade for both spinning and stationary cases calculated with mesh element size of 0.07m and blade total number of elements equals 72562 elements.

The first 10 modes and the corresponding natural frequencies of the Sandia blade rotating at 54 rpm constant rotational velocity have been calculated, and the results for the natural frequencies are indicated in table 2.1, and the modes are shown in figures 2.6 to 2.15.

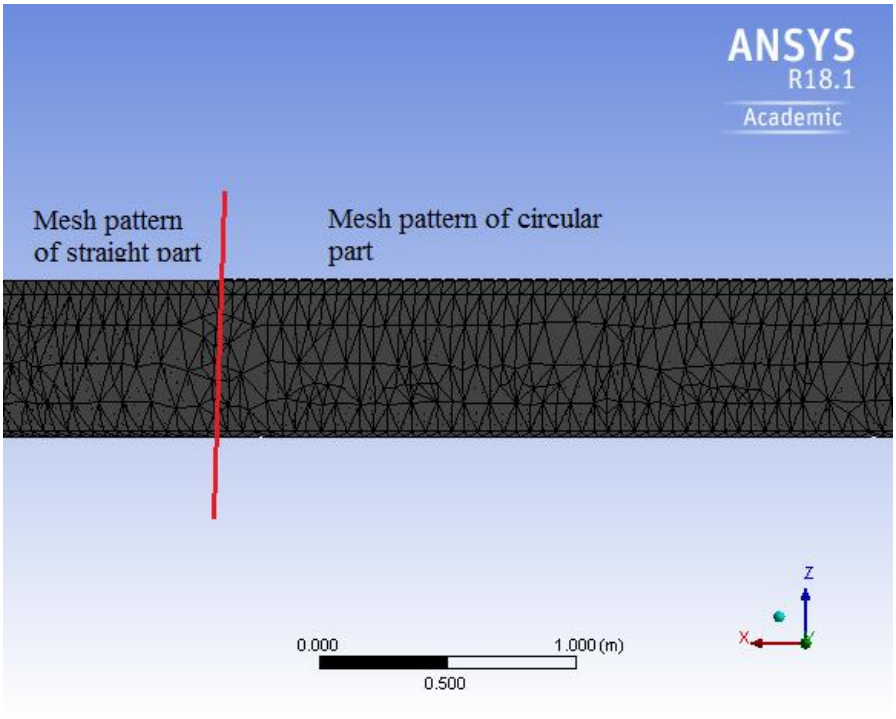

Figure 2.5 17 m diameter Sandia blade meshing pattern

Table 2.1.first 10 natural frequencies of 17 m diameter Sandia blade

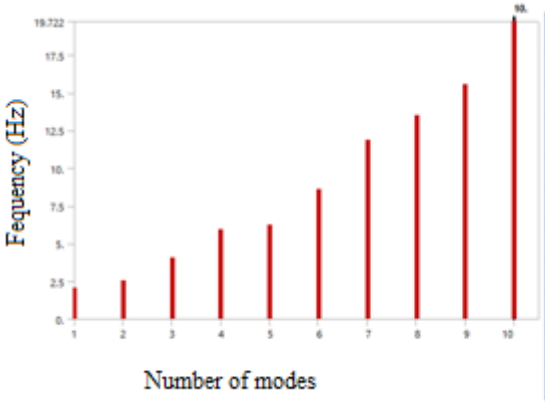

Mode	Frequency [Hz]
1.	2.0416
2.	2.5621
3.	4.0247
4.	5.9241
5.	6.224
6.	8.6015
7.	11.88
8.	13.486
9.	15.57
10.	19.722

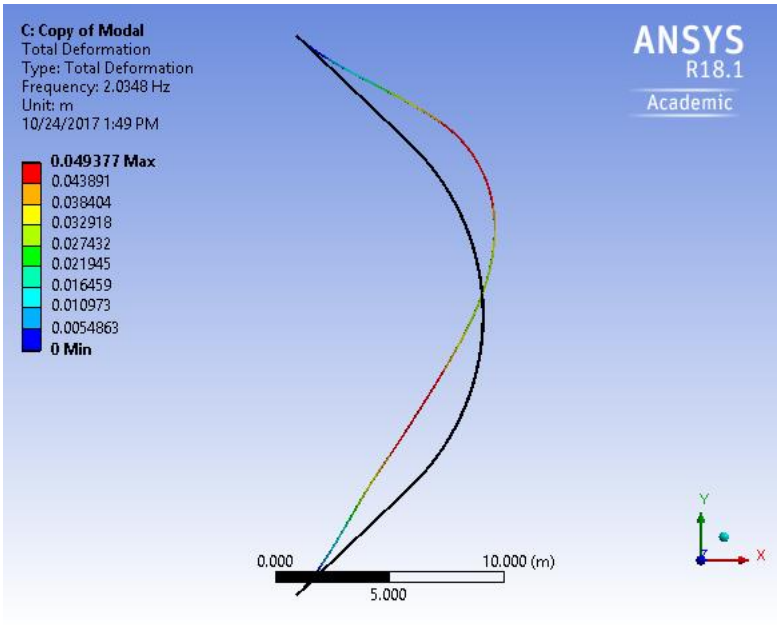

Figure 2.6 first mode of Sandia blade at 54 rpm (flat-wise only), 2.0348 Hz

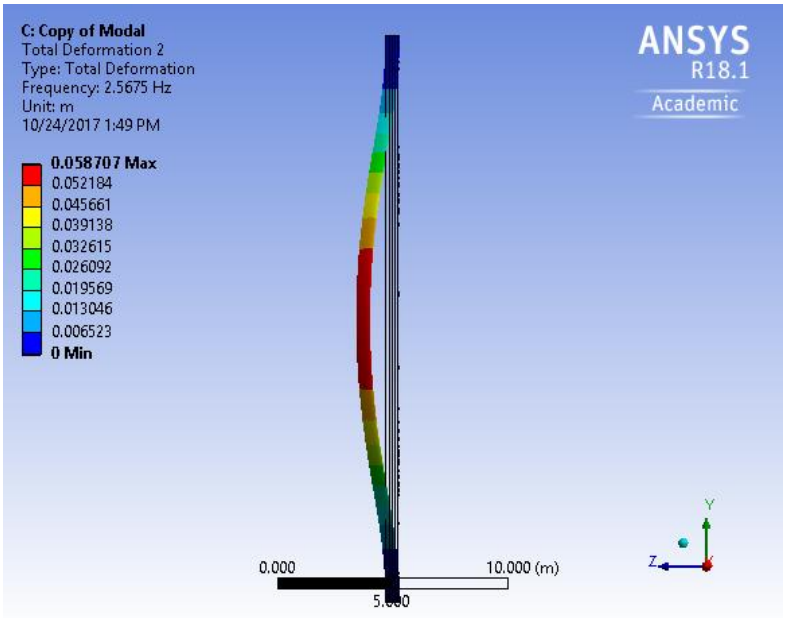

Figure 2.7 second mode of Sandia blade at 54 rpm (edge-wise only), 2.5675 Hz

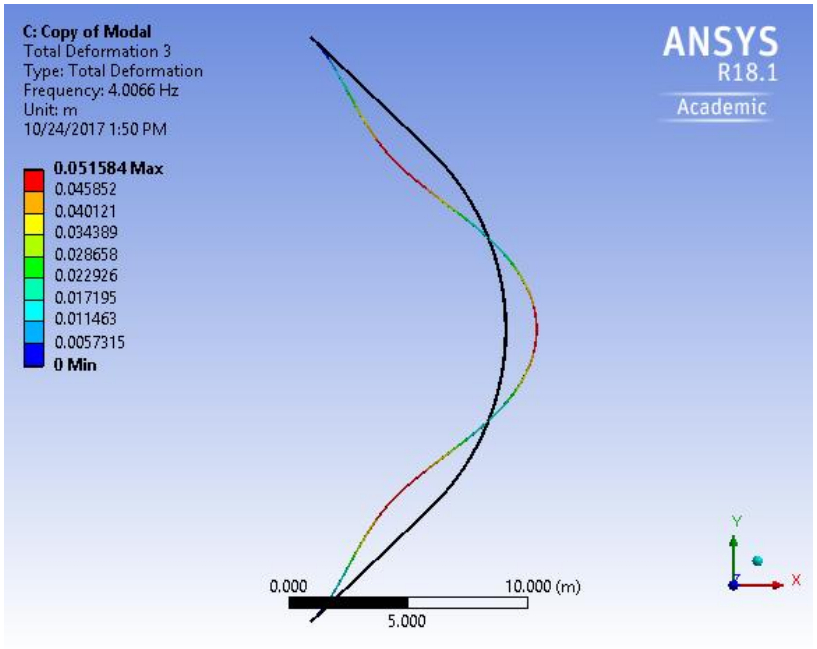

Figure 2.8 third mode of Sandia blade at 54 rpm (flat-wise only), 4 HZ

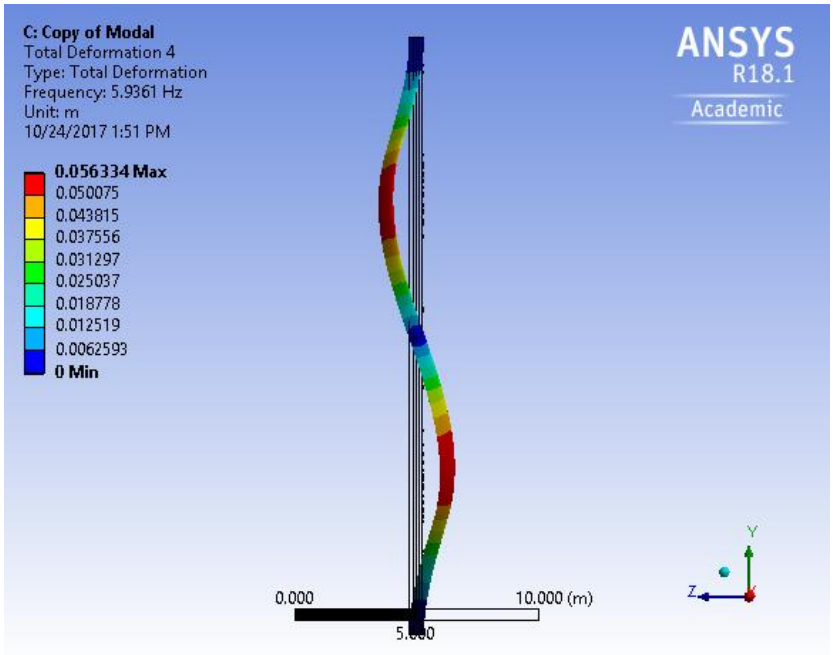

Figure 2.9 fourth mode of Sandia blade at 54 rpm (edge-wise and torsion), 5.94 Hz

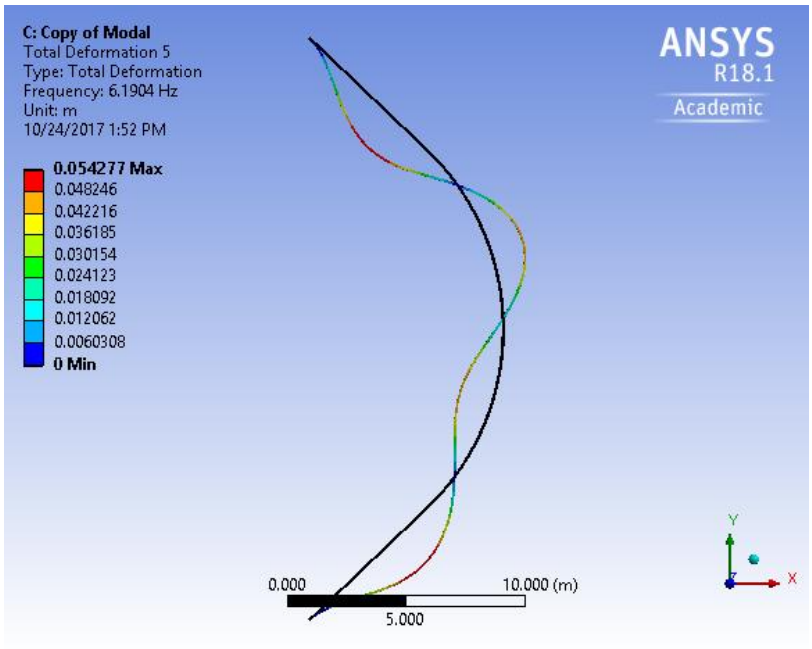

Figure 2.10 fifth mode of Sandia blade at 54 rpm (flat-wise only), 6.1904 Hz

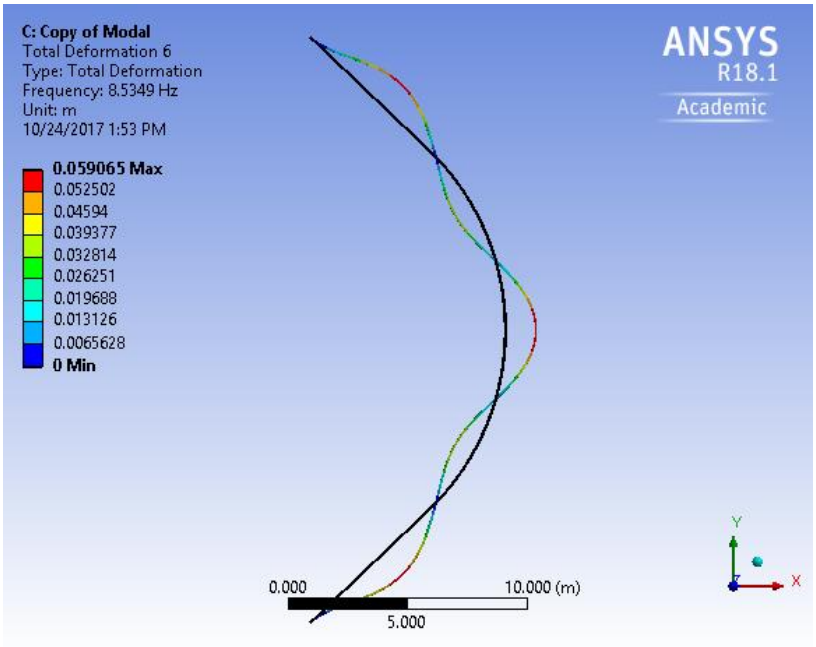

Figure 2.11 sixth mode of Sandia blade at 54 rpm (flat-wise only), 8.5349 Hz

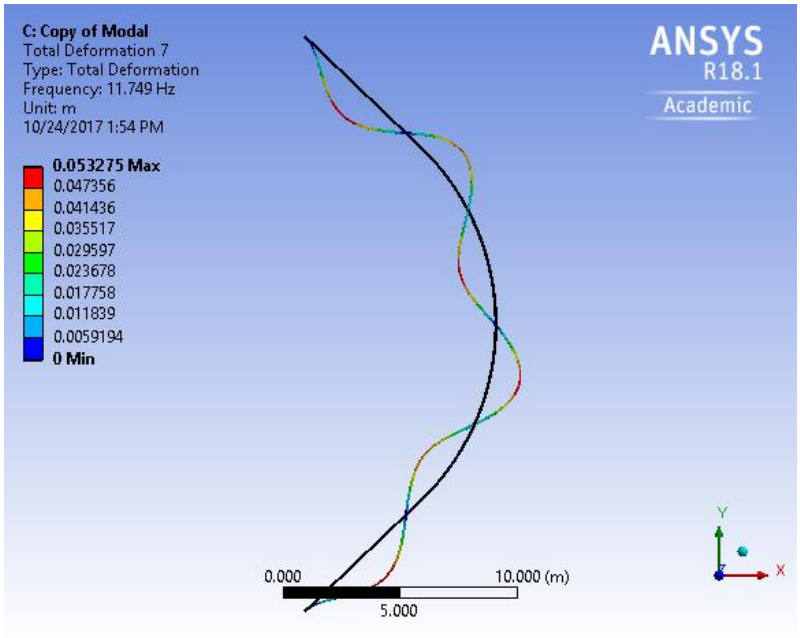

Figure 2.12 seventh mode of Sandia blade at 54 rpm (flat-wise only), 11.749 Hz

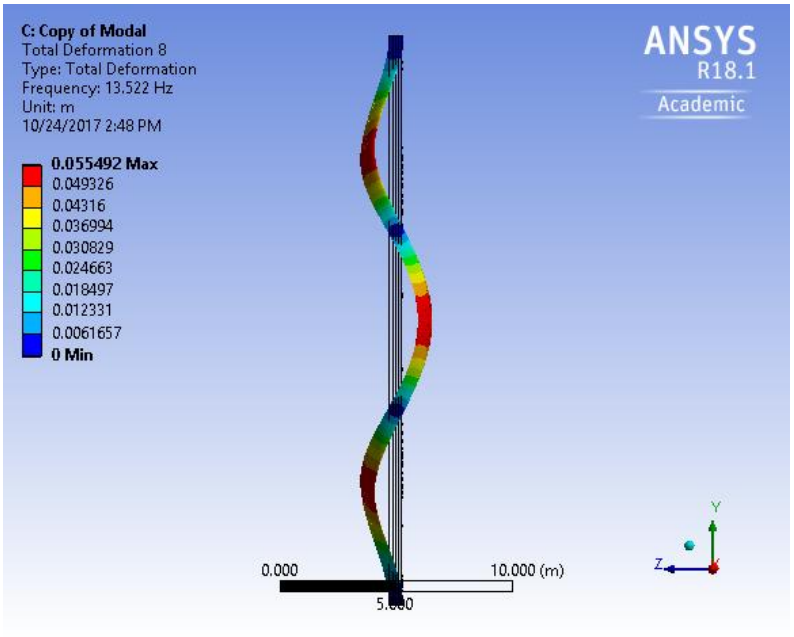

Figure 2.13 eighth mode of Sandia blade at 54 rpm (edge-wise and torsion), 13.52 Hz

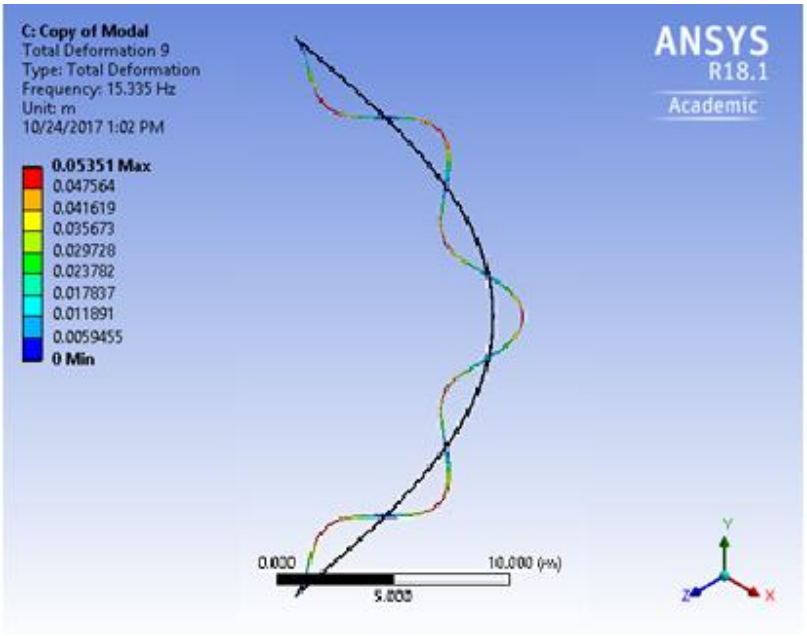

Figure 2.14 ninth mode of Sandia blade at 54 rpm (flat-wise only), 15.335 Hz

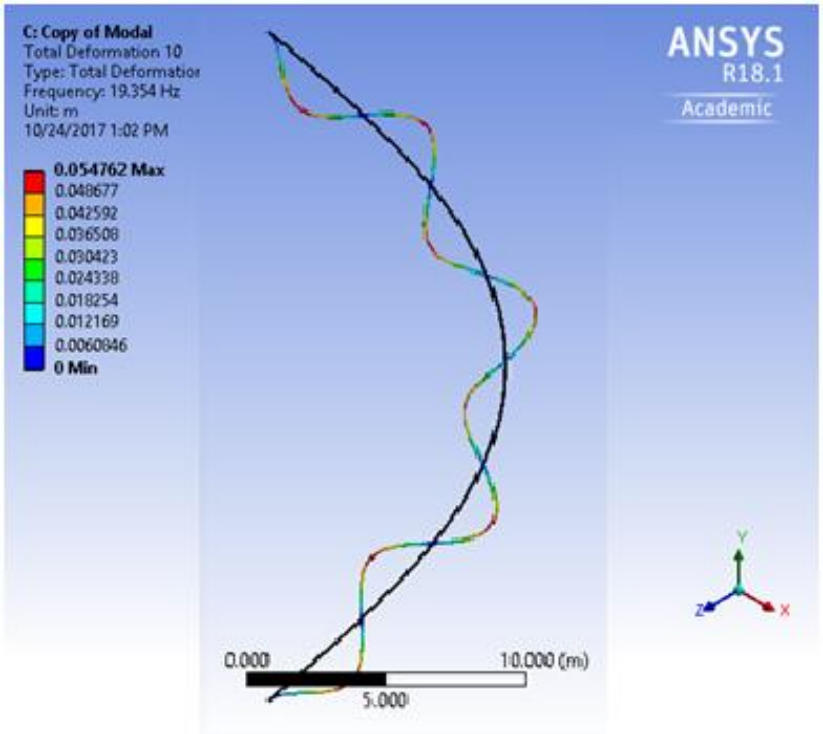

Figure 2.15 tenth mode of Sandia blade at 54 rpm (flat-wise only), 19.354 Hz

Comparing the above results to Sandia results [11] shown in figure 2.16; we find that the results are approximately the same. This validates the finite element analysis based on the ANSYS WORKBENCH and SOLID 187 element, which will then be applied to stationary and ideal troposkein blades.

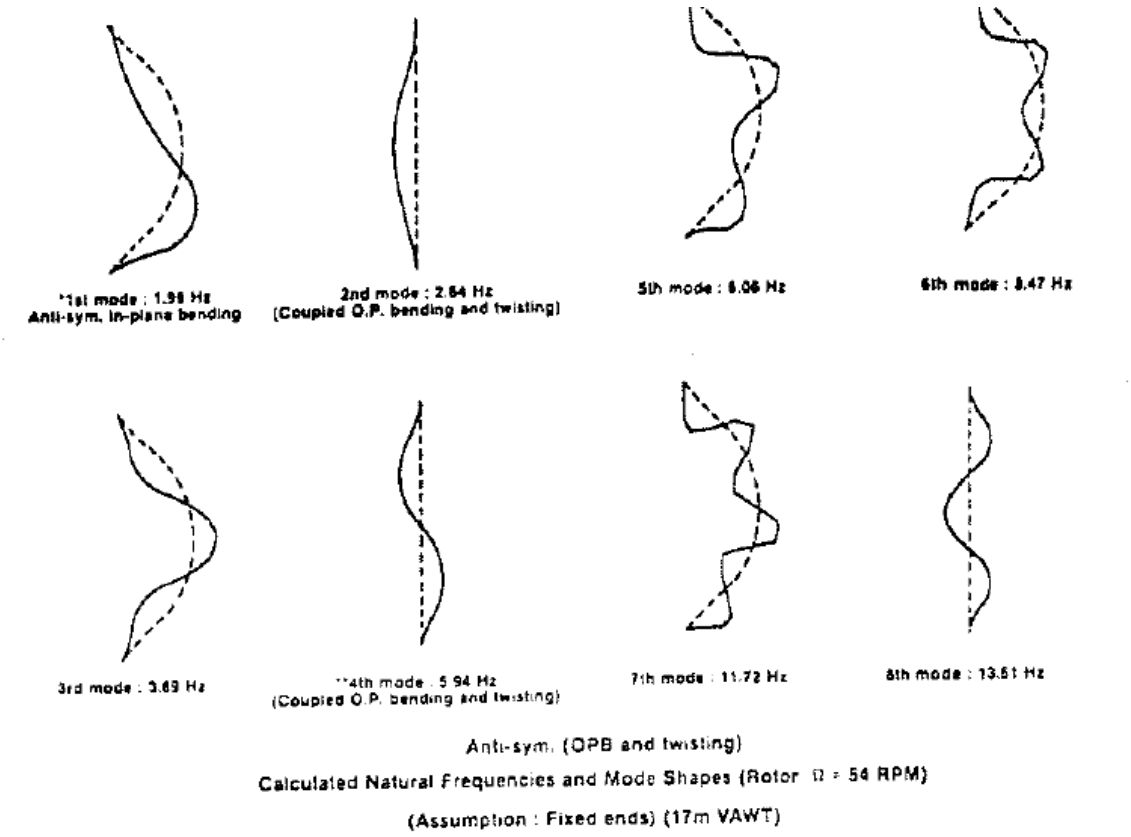

Figure 2.16 mode shapes and frequencies of a single blade of a spinning rotor by Sandia

We can make some observations from these results. Figures 2.6 and 2.10 show antisymmetric flat-wise bending modes. The zero-point on these mode shapes is not exactly centered. Indeed, observing animations shows that the zero point moves during pure modal vibrations. Since the stiffness and mass matrices are symmetric, this zero point shifting suggests that these flat-wise modes also involve extension. This will be

investigated later with both finite-elements and beam-based modeling. The Sandia results also suggest this behavior. Also, the dominantly flat-wise (or possibly flat-wise/extension) and edge/torsion mode shapes suggests that the flat-wise and extension deformation coordinates may be nearly decoupled from the edge-wise and torsion deformation coordinates. A flatwise mode similar to a first mode of a clamped-clamped beam does not show up among the lower modes. Such a mode of flatwise deformation will necessarily involve significant extension and compression. Since extension is in a stiff orientation of a blade (axial deformation tends to be stiffer than bending), such a mode is likely to have a high frequency.

2.4 FEM model for 17m diameter stationary blade of straight-circular-straight shape

We have validated our model by comparing the calculated mode shapes and corresponding modal frequencies of the Sandia shape spinning blade to those which were calculated by Sandia. Now we will consider the mode shapes and modal frequencies of the same blade analyzed in section 2.3 but under stationary conditions, which means the blade rotational velocity is zero. For brevity the mode shapes will not be plotted. For the same element size and meshing pattern, the stationary case modal analysis results can be summarized as shown in table 2.2 below.

Table 2.2 Sandia (MSU) stationary blade first ten modal frequencies

Mode No.	**Freqency**	**shape**
1	1.2824	Flat-wise
2	2.4595	Edge-wise
3	2.8691	Flat-wise

Table 2.2 (cont'd)		
4	4.8445	Flat-wise
5	5.6198	Edge/torsion
6	7.1157	Flat-wise
7	10.188	Flat-wise
8	13.177	Edge/torsion
9	13.693	Flat-wise
10	17.649	Flat-wise

2.5 FEM model for 17m diameter ideal troposkein shaped blade

In this part a modal analysis has been done for an ideal troposkein shape blade with 17 m diameter and blade cross section as in figure 2.17. Here the cross section is a little bit different than the simplified Sandia shape blade to overcome the limitations of the number of elements in the ANSYS software academic version available in our lab at Michigan State University.

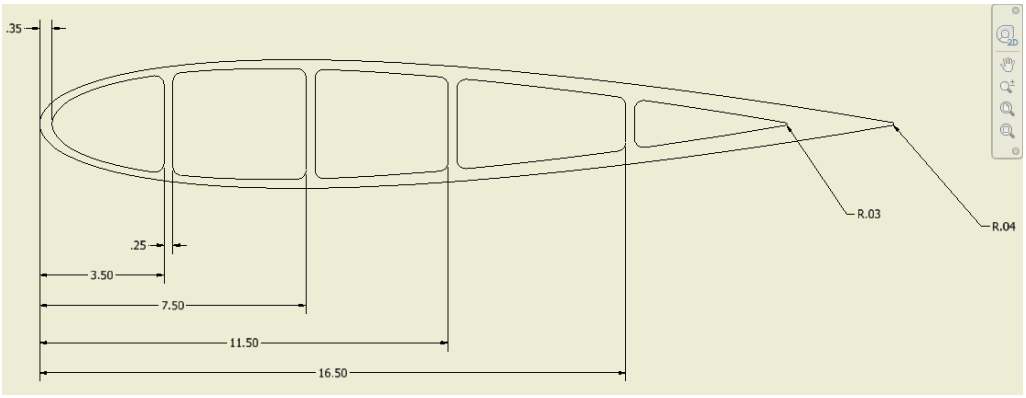

Figure 2.17 NASA 0015 blade cross section for 17 m diameter ideal troposkein shape blade

Comparing the ideal troposkein blade cross section shown in 2.17 to the simplified Sandia blade cross section shown in figure 2.2 we can summarize the differences as in table 2.3 below.

Table 2.3 cross sectional properties for both Sandia and Ideal troposkein blades under discussion

Property	**Sandia cross section**	**Ideal troposkein cross section**
Airfoil / chord length	NASA 0015/0.61 m	NASA 0015/ 0.61m
Cross section area	$0.98 * 10^{-2}\text{m}^2 = 15.129\ \text{in}^2$	$0.96613 * 10^{-2}\text{m}^2 = 14.975\ \text{in}^2$
Flat wise moment of inertia	$0.859 * 10^{-5}$m^4	$0.819 * 10^{-5}$m^4
Edge wise moment of inertia	$2.814 * 10^{-4}$m^4	$2.816 * 10^{-4}$m^4
Total mass of 17 m diameter blade	810.82 Kg	802 Kg
Blade material	6063-T6 Aluminum alloy	6063-T6 Aluminum alloy

From table 2.3 we can see some differences in the blade total mass and edge wise moment of inertia and we see later how these differences will contribute in the comparison of modal analysis results for both blades

2.5.1 3-D model for ideal troposkein shape blade

2.5.1.1 Blade profile

The troposkein shape shown in figure 2.18 can be described by [6]

$$\frac{z_0}{0.5H} = 1 - \frac{F(k_e;\phi)}{F(k_e;\frac{\pi}{2})} \qquad (2.2)$$

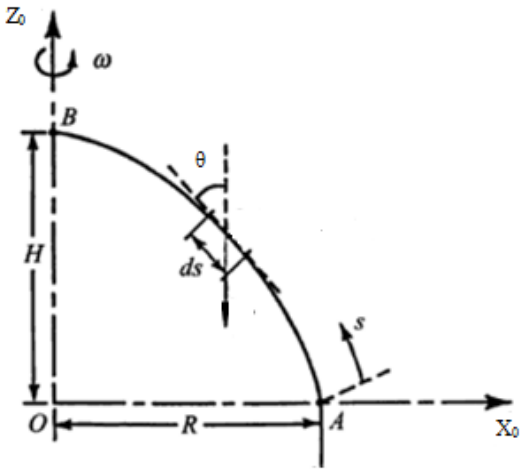

Figure 2.18 Troposkein shape

where

H is the blade height

$\phi = ArcSin[\frac{x_0}{R}]$, where ϕ ranges from 0 to $\frac{\pi}{2}$, R is the blade radius

$F(k_e; \phi)$ is the incomplete elliptic integral of the first kind

$F(k_e; \frac{\pi}{2})$ is the complete elliptic integral of the first kind

2.5.1.2 Elliptic integral arguments

k_e is elliptic integral arguments [6] and it can be calculated from

$$\beta = \frac{2k_e}{1-k^2} * \frac{1}{F(k_e; \frac{\pi}{2})} \qquad (2.3)$$

In Eq. 2.3 $\beta = \frac{R}{H}$.

Solving Eq. (2.3) using Matlab for R=8.5m and H=24.476 gives k_e =0.457

2.5.1.3 Blade length

The blade length can be calculated from k_e and the blade height $2H$ [6] as in Equation 2.4

$$\frac{L}{2H} = \frac{2}{1-K^2} * \frac{E(k_e;\frac{\pi}{2})}{F(k_e;\frac{\pi}{2})} - 1 \qquad (2.4)$$

Solving Eq. 2.4 using MATLAB for *2H*=24.476 m and *k*=0.457 gives *L*=30.42 m which is approximately the same length of Sandia 17 m diameter simplified shape discussed in sections 2.2 and 2.3. Plotting Eq. (2.2) for x_0 ranging from *0* to *R* on MATLAB, where *R*=8.5 and *H*=12.238 m, gives half of the blade shape, as in figure 2.19. The 3-D blade model can be generated by combining the blade cross section figure 2.17 and blade profile figure 2.19.

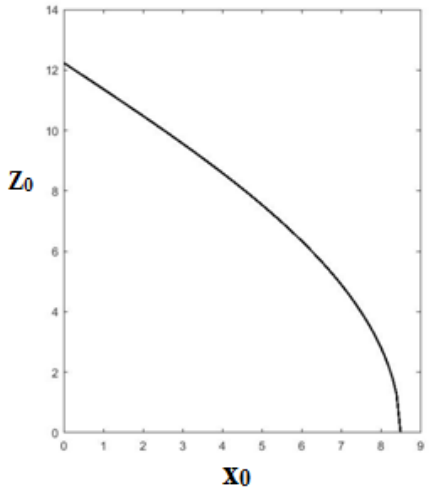

Figure 2.19 17 m diameter troposkein shape with *H*= 12.238 m

2.5.2 FEM modal analysis for 17m diameter blade with ideal troposkein shape

A modal analysis for 17 m diameter ideal troposkein shape blade has been done using ANSYS WORKBENCH by meshing the blade structure using SOLID 187 element and clamping both ends of the blade except for rotation. The blade assumed to be rotating at constant rotational velocity of 54 rpm. The mesh pattern used here is the same as the mesh pattern used for simplified Sandia blade shape to compare the results of both blades significantly.

The first 10 modes and the corresponding natural frequencies of the blade have been calculated and the results for the natural frequencies indicated in table 2.4 and the modes in figures 2.20 to 2.29. The stationary ideal troposkein shaped blade was also analyzed and the modal frequencies are listed in table 2.5, but the mode shapes are not shown for brevity

Table.2.4.first 10 natural frequencies of 17 m diameter ideal troposkein shape blade

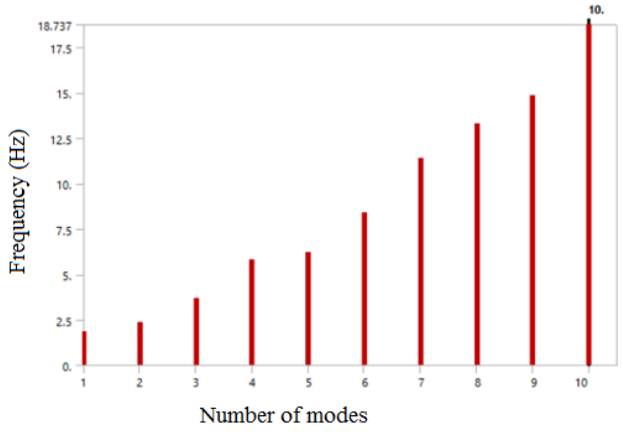

Mode	Frequency [Hz]
1.	1.8665
2.	2.3412
3.	3.68
4.	5.8174
5.	6.1824
6.	8.363
7.	11.36
8.	13.301
9.	14.821
10.	18.737

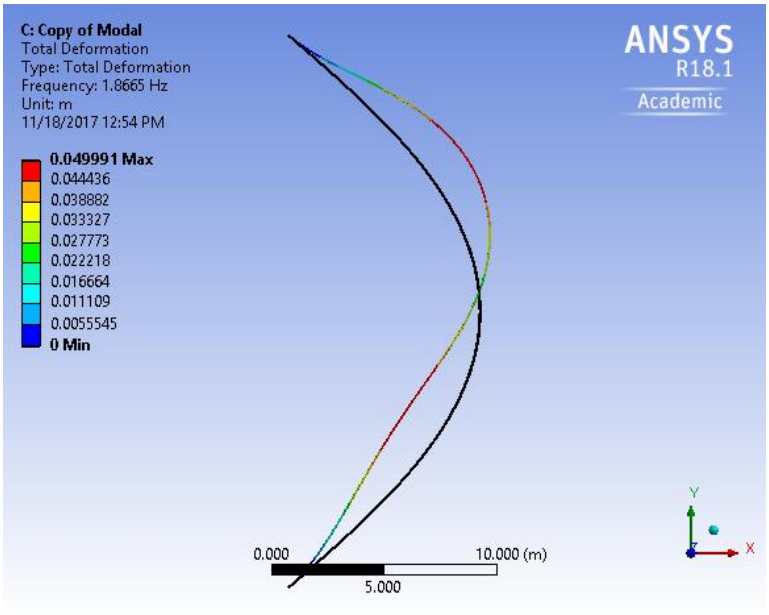

Figure 2.20 first mode for the troposkein blade at 54 rpm (flat-wise only), 1.87 Hz

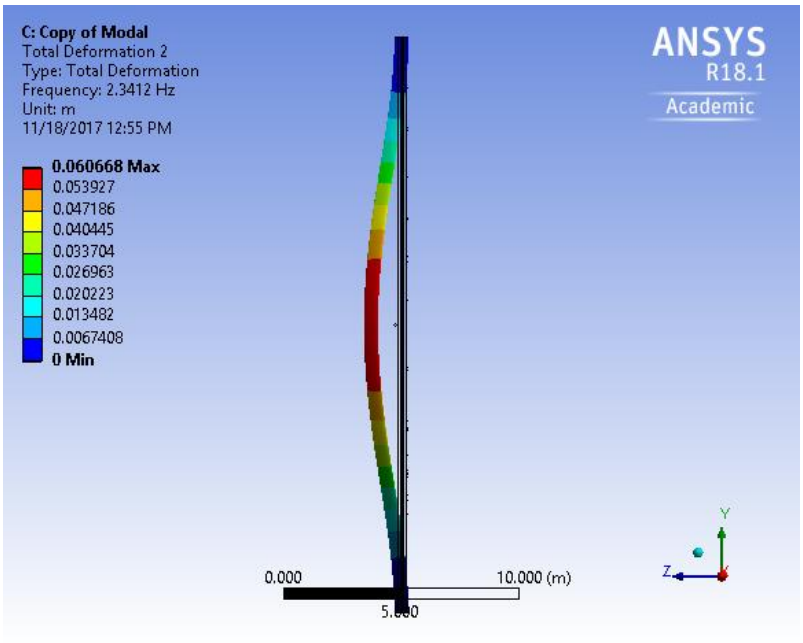

Figure 2.21 second mode for the troposkein blade at 54 rpm (edge-wise only), 2.34 Hz

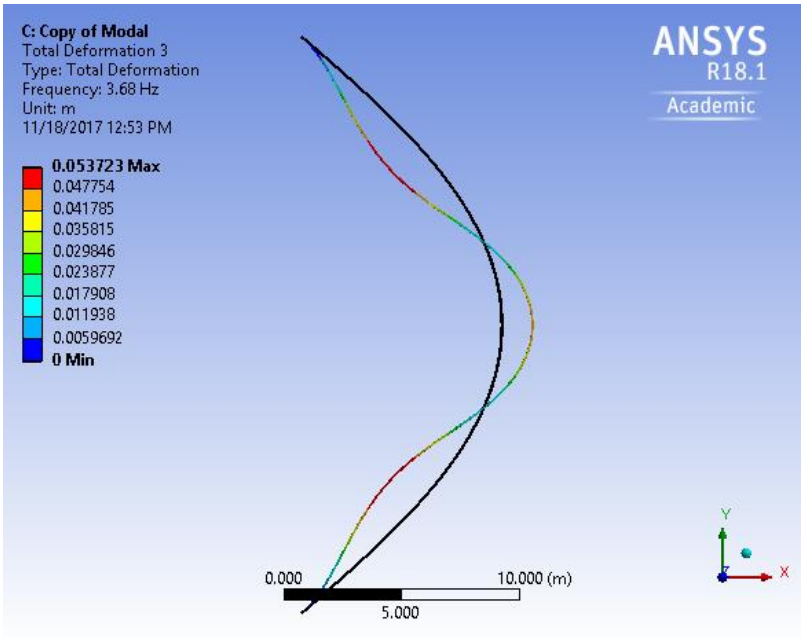

Figure 2.22 third mode for the troposkein blade at 54 rpm (flat-wise only), 3.68 Hz

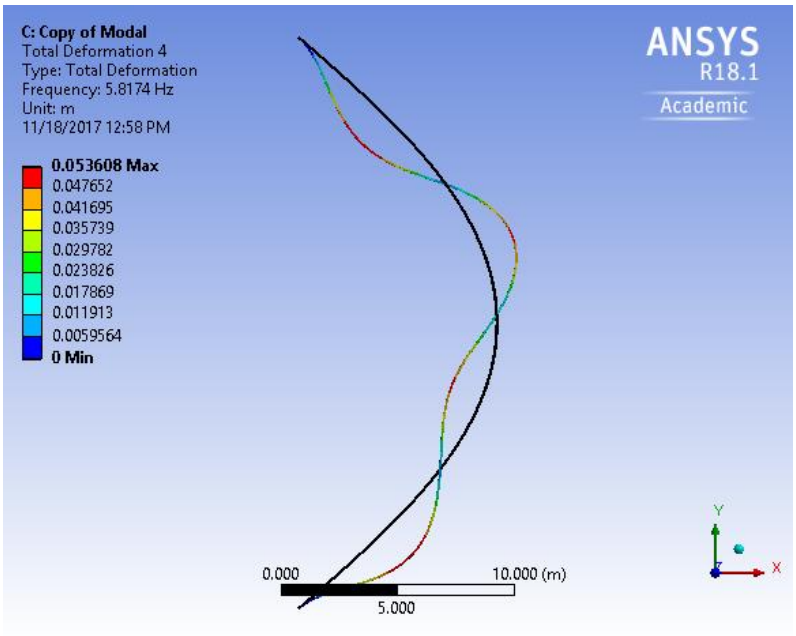

Figure 2.23 fourth mode for the troposkein blade at 54 rpm (flat-wise only), 5.82 Hz

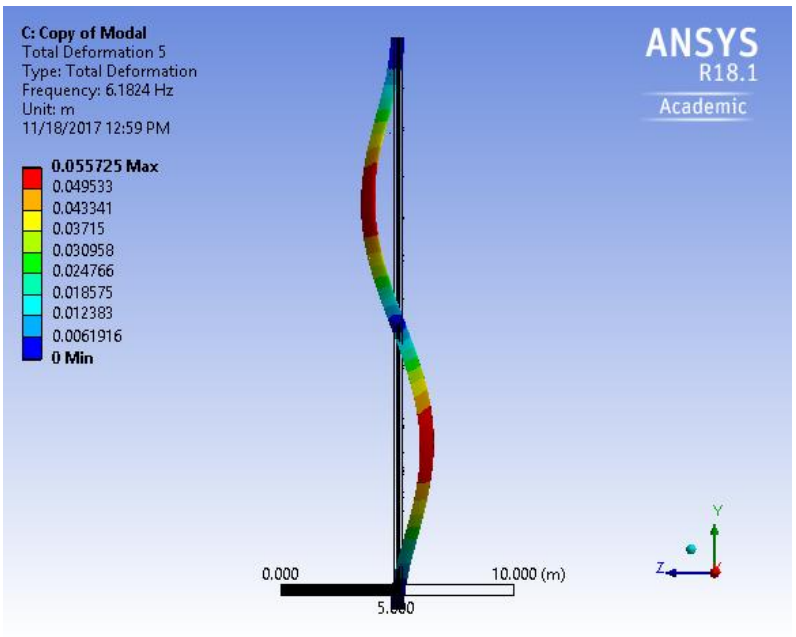

Figure 2.24 fifth mode for the troposkein blade at 54 rpm (edge-wise & torsion), 6.2 Hz

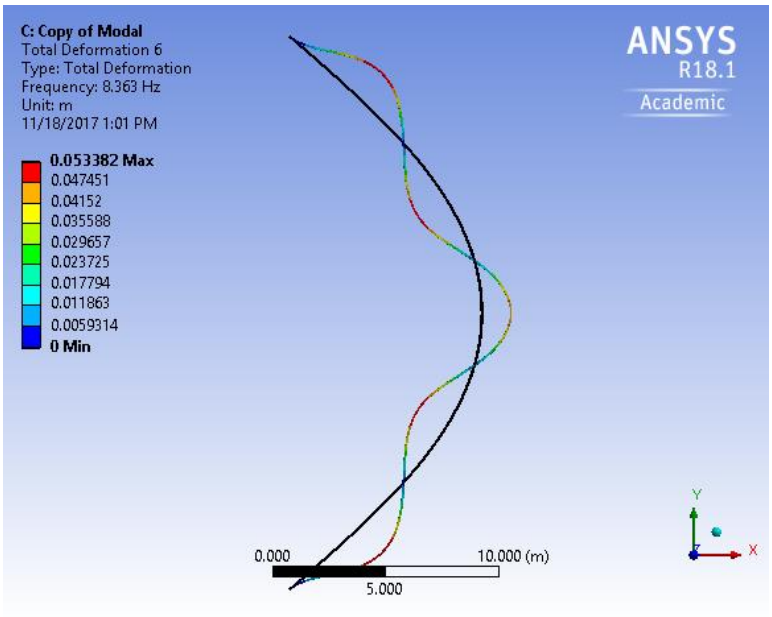

Figure 2.25 sixth mode for the troposkein blade at 54 rpm (flat-wise only), 8.4 Hz

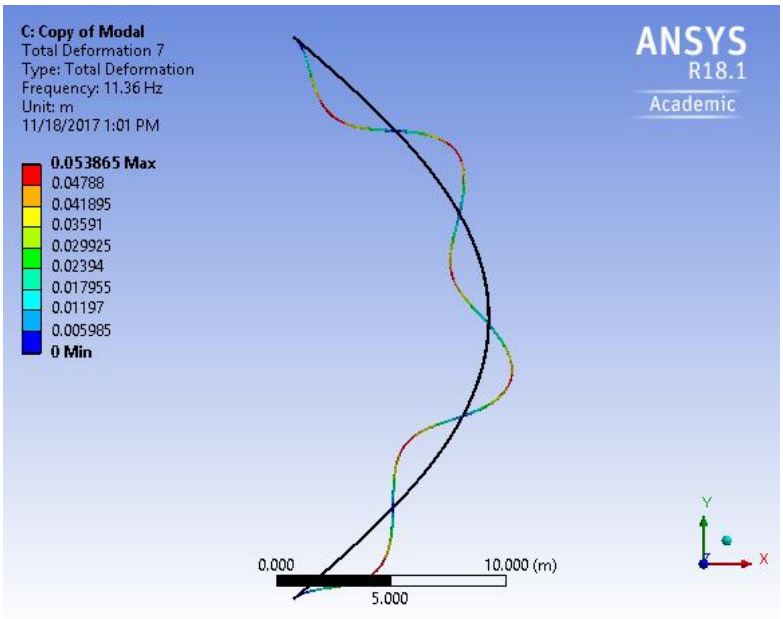

Figure 2.26 seventh mode for the troposkein blade at 54 rpm (flat-wise only), 11.36 Hz

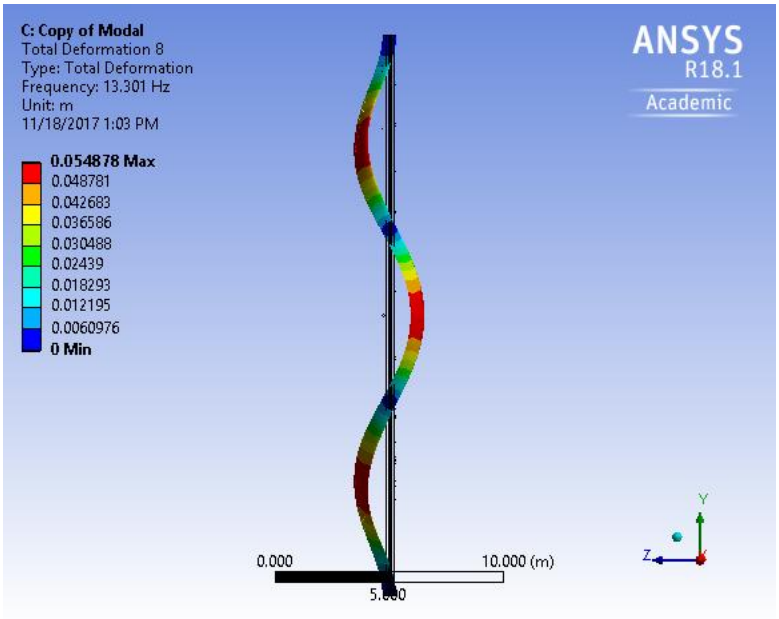

Figure 2.27eighth mode for the troposkein blade at 54 rpm (edge-wise / torsion), 13.3 Hz

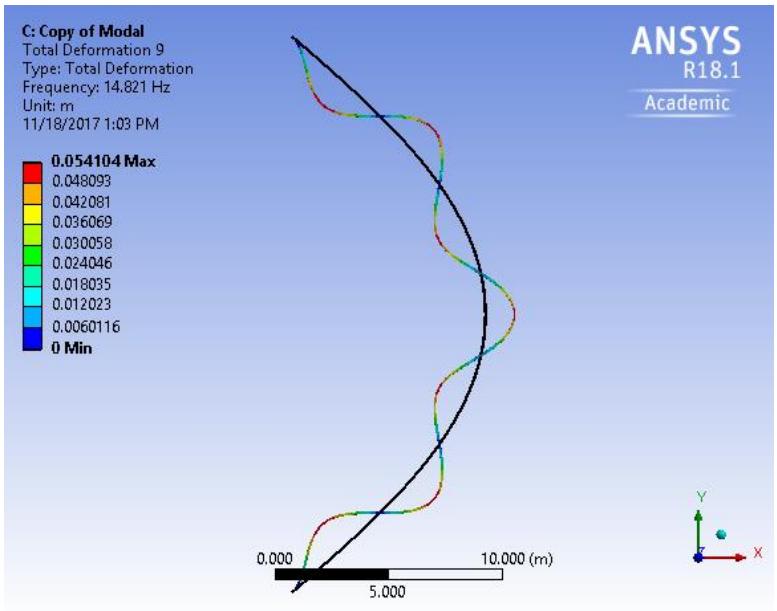

Figure 2.28 ninth mode for the troposkein blade at 54 rpm (flat-wise only), 14.82 Hz

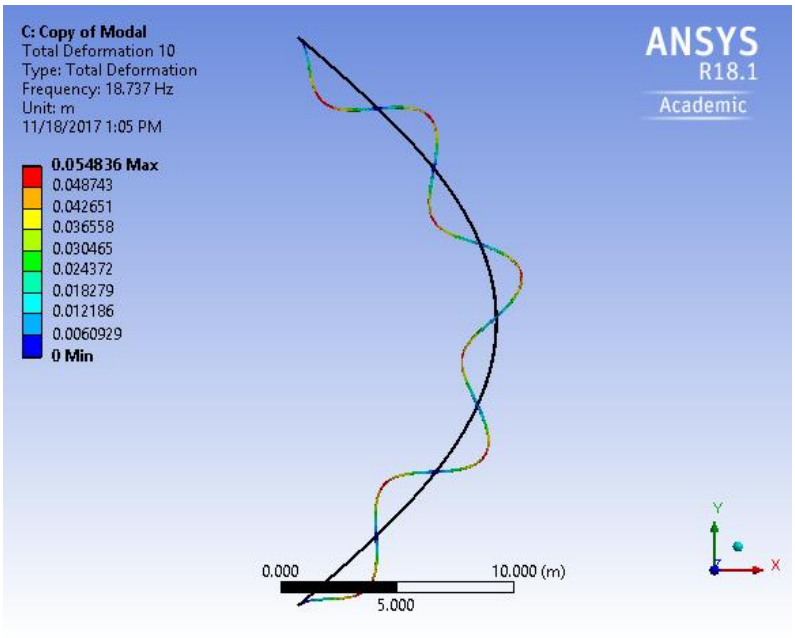

Figure 2.29 tenth mode for the troposkein blade at 54 rpm (flat-wise only), 18.74 Hz

Table 2.5. Comparison of the lower modal frequencies as obtained by finite element analysis. "Sandia" refers to the straight-circular-straight blade model. Spinning occurs at 54 rpm. F (flat-wise), E (edge-wise), and ET (edge-wise/ torsion)

Mode #	Sandia(54 rpm)		Sandia (MSU) 54rpm		Troposkein 54 rpm		Sandia (MSU) stationary		Troposkein (stationary	
	Freq.	shape	Freq.	shape	Freq.	shape	Freq.	shape	Freq.	shape
1	1.99	F	2.04	F	1.87	F	1.28	F	1.28	F
2	2.54	E	2.57	E	2.34	E	2.46	E	2.3	E
3	3.69	F	4	F	3.68	F	2.87	F	2.81	F
4	5.94	ET	5.94	ET	5.82	F	4.85	F	4.78	F
5	6.06	F	6.2	F	6.2	ET	5.62	ET	5.6	ET
6	8.47	F	8.54	F	8.36	F	7.12	F	7.21	F
7	11.72	F	11.75	F	11.36	F	10.2	F	10.14	F
8	13.51	ET	13.52	ET	13.3	ET	13.2	ET	13.06	ET
9			15.34	F	14.82	F	13.7	F	13.55	F
10			19.354	F	18.737	F	17.65	F	17.43	F

Table 2.5 summarizes our results for comparing the FEA results of Sandia blade and ideal troposkein blade for both stationary and rotating condition with constant rotational velocity 54 rpm as follows.

1. For the spinning case of the simplified blade we find that our finite element model results and Sandia finite element results are essentially the same.
2. Comparing the spinning blade (54 rpm) first ten modes for ideal troposkein shape and Sandia simplified shape we found that the natural frequencies spinning of ideal troposkein shape is little less than the natural frequencies of Sandia one. This difference may be because the ideal troposkein shape is slightly different, and its cross section is little bit different than the simplified Sandia shape blade to overcome the limitations of the number of elements in the ANSYS software academic version available in our lab, which makes the ideal troposkein shaped blade is little lighter than the Sandia one.
3. For stationary free vibration case the first ten mode shapes for Sandia and ideal troposkein shapes are essentially the same, but the natural frequencies of ideal troposkein shape are a little lower than for simplified Sandia shape. This difference in modal frequencies may be because of the difference in profile or difference in cross section to overcome the ANSYS limitation problem as we mentioned before.
4. The spinning blades have increased modal frequencies. The increase is more significant in the flat-wise modes than the edge-wise/torsion modes. It is likely that the spin stiffening induces tension in the blade, and has a more significant effect on flat-wise bending than torsion. Since the flat-wise modal frequencies undergo larger changes under spin, in some cases their frequencies become larger than a nearby edge/torsion mode, and the modal ordering therefore changes slightly.

3 Chapter 3: Analytical beam-based formulation of troposkein shaped blade modal analysis

3.1 Introduction

In this chapter we will study the vibration of Darrieus wind turbine blade with a troposkein-shape. Because of the blade shape complexity we will use an assumed modes method for discretizing the kinetic energy and potential energy for the case of free vibration (no aerodynamic forces condition). The gravitational effect will be neglected and Lagrange's equation will be used to formulate the mass and stiffness matrices which can then be used to calculate the natural frequency and mode shapes analytically.

In the current work we will use the clamped-clamped beam modes as our assumed modal functions to formulate the displacement functions for the blade, and by substituting these functions and their derivatives we can get descretized expressions for the energies, which can be used to approximate the modes and frequencies.

3.2 Blade potential energy

The potential energy of the blade can be divided in to two parts:

1. Strain energy
2. Gravitational potential energy or gravitational work

Here we will consider the strain energy only. The gravitational potential energy will be neglected in this initial study. The strain energy SE for an element of volume V can be expressed as

$$SE = \frac{1}{2} V \sigma \epsilon \qquad (3.1)$$

where

V is the volume

σ is the engineering stress

ϵ is the engineering strain

To express the blade strain energy using equation (3.1), several orthogonal coordinate systems will be employed. These coordinate systems are shown in figures 3.1, 3.2, and 3.3 and can be defined as follows

1. Inertial coordinate system ($X_I\ Y_I\ Z_I$ - system). As shown in figure 3.1 the Z_I-axis coincides with the vertical axis of the rotor. The X_I-axis aligned with the free stream wind velocity, V_∞. The Y_I-axis is normal to X_I-Z_I plane.
2. Rotating coordinate system ($X_R\ Y_R\ Z_R$ - system). As shown in figure 3.1, this system is obtained by rotating the $X_I\ Y_I\ Z_I$ – system by an angle $\tau = \Omega * t$, where Ω is the turbine rotational velocity.
3. Blade coordinate system B1 ($X_{B1}Y_{B1}Z_{B1}$-system) ; as shown in figure 3.1 this blade local coordinate system has its origin coincident with the blade cross section shear center and parallel to the $X_R\ Y_R\ Z_R$ – system. The unit vectors of this system are $\bar{e}_{x_{\mathrm{B1}}}, \bar{e}_{y_{\mathrm{B1}}}, \bar{e}_{z_{\mathrm{B1}}}$ in X_{B1}, Y_{B1}, Z_{B1} respectively
4. Blade coordinate system B2 ($X_{B2}Y_{B2}Z_{B2}$-system). As shown in figure 3.1, this system is obtained by rotating the B1 system about the negative Y_{B1}-axis by an angle θ (θ is the meridian angle, which we will discuss later in detail). The unit vectors of this system are $\bar{e}_{x_{\mathrm{B2}}}, \bar{e}_{y_{\mathrm{B2}}}, \bar{e}_{z_{\mathrm{B2}}}$ in X_{B2}, Y_{B2}, Z_{B2}, respectively.
5. Blade principle axes system B3 ($X_{B3}Y_{B3}Z_{B3}$-system). As shown in figure 3.2, in this coordinate system X_{B3} and Y_{B3} are taken to be aligned with the minor and major

principle axes of the blade cross section, respectively. The unit vectors of this system are $\bar{e}_{x_{B3}}, \bar{e}_{y_{B3}}, \bar{e}_{z_{B3}}$ in X_{B3}, Y_{B3}, Z_{B3}, respectively.

6. The blade coordinate system B6 ($X_{B6}Y_{B6}Z_{B6}$-system) is shown in figure 3.3 and is obtained by translating and rotating the B3-system as we will see later in this chapter.
7. The deformations of the blade elastic axis are denoted by *u, v,* and *w,* in the X_{B3}, Y_{B3}, Z_{B3} respectively, and ϕ represents the twisting deformation.

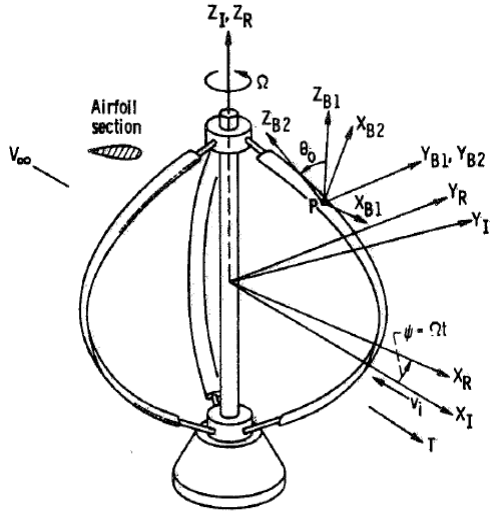

Figure 3.1 vertical-axis wind turbine and coordinate systems [8]

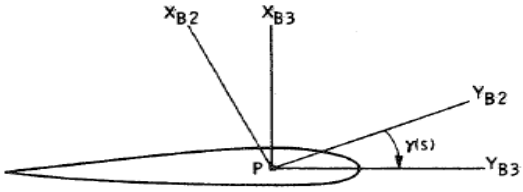

Figure 3.2 coordinate systems of blade cross section [8]

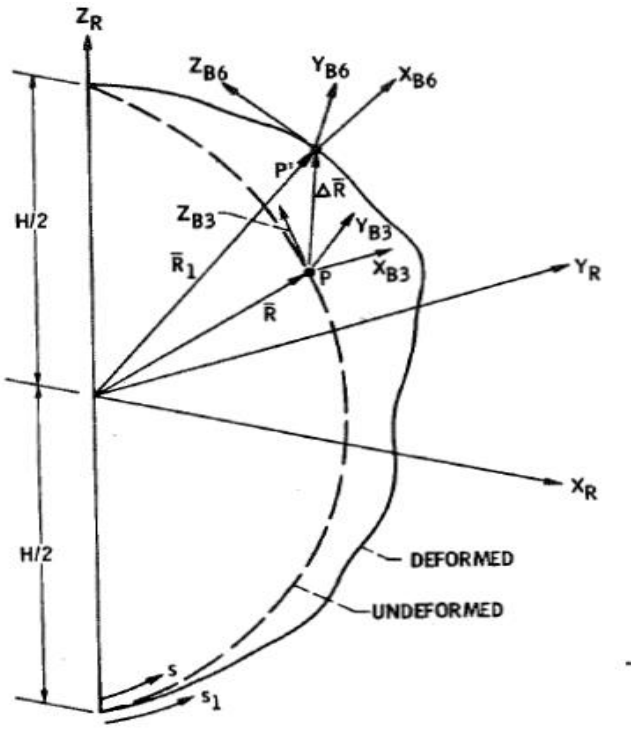

Figure 3.3 axis of blade before and after deformation, and coordinate systems [8]

The blade strain energy can be expressed based on eq. (3.1) and using the B3 coordinate system as

$$SE = \frac{1}{2}\int_0^S \int_0^{Y_3} \int_0^{X_3} (\sigma_{z_3z_3}\gamma_{z_3z_3} + \sigma_{z_3x_3}\gamma_{z_3x_3} + \sigma_{z_3y_3}\gamma_{z_3y_3})\, dx_3\, dy_3\, dz_3 \qquad (3.2)$$

Here because of the blade slenderness assumption we neglected $\gamma_{x_3x_3}$, $\gamma_{x_3y_3}$, and $\gamma_{y_3y_3}$. Assuming that the engineering strain components $\gamma_{z_3z_3}, \gamma_{z_3x_3}, \gamma_{z_3y_3}$ are equal to the corresponding components of Lagrangian strain $\epsilon_{z_3z_3}, \epsilon_{z_3x_3}, \epsilon_{z_3y_3}$, and using Hooke's law we can get

$$\sigma_{z_3z_3} = E\gamma_{z_3z_3} = E\epsilon_{z_3z_3}$$

$$\sigma_{z_3x_3} = G\gamma_{z_3x_3} = 2G\epsilon_{z_3x_3} \qquad (3.3)$$

$\sigma_{z_3y_3} = G\gamma_{z_3y_3} = 2G\epsilon_{z_3y_3}$

Also

$\gamma_{z_3z_3} = \epsilon_{z_3z_3}$

$\gamma_{z_3x_3} = 2\epsilon_{z_3x_3}$ (3.4)

$\gamma_{z_3y_3} = 2\epsilon_{z_3y_3}$

Substituting equations (3.3) and (3.4) into (3.2), we get

$$SE = \frac{1}{2}\int_0^S \int_0^{Y_3} \int_0^{X_3} (E\epsilon_{z_3z_3}^2 + 4G(\epsilon_{z_3x_3}^2 + \epsilon_{z_3y_3}^2))\, dx_3\, dy_3\, dz_3 \qquad (3.5)$$

From eq. (3.5) we can find that the blade strain energy is only a function of Lagrangian strain components $\epsilon_{z_3z_3}, \epsilon_{z_3x_3}, \epsilon_{z_3y_3}$. So we need to calculate these strain components for the troposkein shaped blade.

3.2.1 Derivation of strain equations

From continuum mechanics we know that the Lagrangian finite strain ϵ for a beam of length L subjected to axial stress is given by [20]

$\epsilon = \frac{1}{2}(\frac{l^2 - L^2}{L^2})$ (3.6)

where

l is the extended length

From eq. (3.6) we can express the strain tensor for the blade as

$\epsilon_{ij} = \frac{1}{2}(\frac{|d\bar{r}_1|^2 - |d\bar{r}_0|^2}{|d\bar{r}_0|^2})$ (3.7)

where $\bar{r_0}$ and $\bar{r_1}$ are the position vectors of an arbitrary mass point in the cross section of the blade before and after deformation respectively [10] with respect to the origin of the inertial coordinate system ($X_I Y_I Z_I$) as shown in figure 3.1

Rearranging eq. 3.7 we get

$$/d\bar{r}_1/^2 - /d\bar{r}_0/^2 = 2/d\bar{r}_0/^2\epsilon_{ij} \qquad (3.8)$$

Using figures 3.1, 3.2, and 3.3, and assuming that the blade cross section deformation is negligible, using a slender blade assumption we get

$$\bar{r}_0 = \bar{R} + x_3\bar{e}_{x_{B3}} + y_3\bar{e}_{y_{B3}}$$

$$\bar{r}_1 = \bar{R}_1 + x_3\bar{e}_{x_{B6}} + y_3\bar{e}_{y_{B6}} \qquad (3.9)$$

where

1. $\bar{R}$ and $\bar{R}_1$ are the position vectors of the blade cross section shear center (P) before and after deformation with respect to the inertial coordinate system ($X_I Y_I Z_I$) which is shown in figure 3.3.
2. x_3 and y_3 are the coordinates of any arbitrary point in the blade cross section with respect to the coordinate system ($X_{B3}Y_{B3}$) shown in figure 3.2, where in this system X_3 and Y_3 are taken to be coincident with blade cross section minor and major axes, respectively, and $\bar{e}_{x_{B3}}$ and $\bar{e}_{y_{B3}}$ are the unit vectors in the direction of X_{B3} and Y_{B3} respectively.
3. $\bar{e}_{x_{B6}}$ and $\bar{e}_{y_{B6}}$ are position vectors in the directions of X_{B6} and Y_{B6} ,respectively, where X_{B6} and Y_{B6} are the minor and major axes of the blade cross section, respectively, after deformation. We will indicate later how we get the B6- coordinate system from B3-coordinate system.

Now from eq. (3.8) we need the differentials of $\bar{r}_0$ and $\bar{r}_1$. Firstly,

$$d\bar{r}_0 = [\frac{d\bar{R}}{ds} + x_3\frac{d\bar{e}_{x_{B3}}}{ds} + y_3\frac{d\bar{e}_{y_{B3}}}{ds}]ds + \bar{e}_{x_{B3}}dx_3 + \bar{e}_{y_{B3}}dy_3 \qquad (3.10)$$

where *s* is the same as Z_3, and represents a coordinate tangent to the blade elastic axis at each cross section and perpendicular to the cross section minor and major axes. The derivative of the unit vectors with respect to the axial blade coordinate *s* can be written as

$$\frac{d\bar{e}_{x_{B3}}}{ds} = \bar{\omega}_{X_{B3}Y_{B3}Z_{B3}} \times \bar{e}_{x_{B3}}$$

$$\frac{d\bar{e}_{y_{B3}}}{ds} = \bar{\omega}_{X_{B3}Y_{B3}Z_{B3}} \times \bar{e}_{y_{B3}} \qquad (3.11)$$

The curvature vector of the undeformed blade $\bar{\omega}_{X_{B3}Y_{B3}Z_{B3}}$ is given by

$$\bar{\omega}_{X_{B3}Y_{B3}Z_{B3}} = -\theta'\bar{e}_{y_{B2}} + \gamma'\bar{e}_{z_{B3}} \qquad (3.12)$$

where

θ is the blade meridian angle or the angle between the vertical and the tangent to the blade elastic axis at any point.

γ is the total section pitch angle which includes the built-in twist and section pitch change due to control inputs. In this thesis we will consider a blade with zero pitch angle.

From figure 3.2 the coordinate system B2 is the coordinate system generated by rotating the B1-coordinate system by an angle θ about the negative y_{B1}-axis to make the z_{B1}-axis tangent to the blade elastic axis. The transformation matrix between the B2 and B3 coordinate systems is

$$\begin{pmatrix} \bar{e}_{x_{B2}} \\ \bar{e}_{y_{B2}} \\ \bar{e}_{z_{B2}} \end{pmatrix} = \begin{bmatrix} cos\gamma & -sin\gamma & 0 \\ sin\gamma & cos\gamma & 0 \\ 0 & 0 & 1 \end{bmatrix} \begin{pmatrix} \bar{e}_{x_{B3}} \\ \bar{e}_{y_{B3}} \\ \bar{e}_{z_{B3}} \end{pmatrix} \qquad (3.13)$$

Eq. (3.13) gives

$$\bar{e}_{y_{B2}} = \bar{e}_{x_{B3}} \sin\gamma + \bar{e}_{y_{B3}} \cos\gamma \qquad (3.14)$$

Substituting eq. (3.14) in eq. (3.12) gives

$$\bar{\omega}_{X_{B3}Y_{B3}Z_{B3}} = -\theta'\sin\gamma\bar{e}_{x_{B3}} - \theta'\cos\gamma\bar{e}_{y_{B3}} + \gamma'\bar{e}_{z_{B3}} \quad (3.15)$$

Now eq. (3.11) can be written as

$$\frac{d\bar{e}_{x_{B3}}}{ds} = \gamma'\bar{e}_{y_{B3}} + \theta'\cos\gamma\bar{e}_{z_{B3}}$$

$$\frac{d\bar{e}_{y_{B3}}}{ds} = -\gamma'\bar{e}_{x_{B3}} - \theta'\sin\gamma\bar{e}_{z_{B3}} \quad (3.16)$$

Substituting equation (3.16) into equation (3.10) and letting

$$k_{x_{B3}} = -\theta'\sin\gamma$$

$$k_{y_{B3}} = -\theta'\cos\gamma$$

$$k_{z_{B3}} = \gamma'$$

leads to

$$d\bar{r}_0 = \left(dx_3 - y_3 k_{z_{B3}} ds\right)\bar{e}_{x_{B3}} + \left(x_3 k_{z_{B3}} ds + dy_3\right)\bar{e}_{y_{B3}}$$

$$+(1 + y_3 k_{x_{B3}} - x_3 k_{y_{B3}})ds\bar{e}_{z_{B3}} \quad (3.17)$$

With the same procedure as $d\bar{r}_0$ we can express $d\bar{r}_1$ as

$$d\bar{r}_1 = \left(dx_3 - y_3 k_{z_{B6}} ds_1\right)\bar{e}_{x_{B6}} + \left(dy_3 + x_3 k_{z_{B6}} ds_1\right)\bar{e}_{y_{B6}}$$

$$+(1 - x_3 k_{y_{B6}} + y_3 k_{x_{B6}})ds_1\bar{e}_{z_{B6}} \quad (3.18)$$

Now from eq. (3.8) the Lagrangian strain tensor can be defined as follows

$$d\bar{r}_1 . d\bar{r}_1 - d\bar{r}_0 . d\bar{r}_0 = 2[dx_3 dx_3 dz_3][\epsilon_{ij}]\begin{pmatrix} dx_3 \\ dx_3 \\ dz_3 \end{pmatrix} \quad (3.19)$$

$$\epsilon_{ij} = \begin{pmatrix} \epsilon_{x_3x_3} & \epsilon_{x_3y_3} & \epsilon_{x_3z_3} \\ \epsilon_{y_3x_3} & \epsilon_{y_3y_3} & \epsilon_{y_3z_3} \\ \epsilon_{z_3x_3} & \epsilon_{z_3y_3} & \epsilon_{z_3z_3} \end{pmatrix}$$

Expanding the right hand side of eq. (3.19) gives

$$2[dx_3 dx_3 dz_3][\epsilon_{ij}]\begin{pmatrix} dx_3 \\ dx_3 \\ dz_3 \end{pmatrix} = 2(\epsilon_{x_3x_3} {dx_3}^2 + \epsilon_{x_3y_3} dx_3 dy_3 + \epsilon_{x_3z_3} dx_3 dz_3 + \epsilon_{y_3y_3} {dy_3}^2 +$$

$$\epsilon_{y_3x_3} dx_3 dy_3 + \epsilon_{y_3z_3} dy_3 dz_3 + \epsilon_{z_3z_3} {dz_3}^2 + \epsilon_{z_3x_3} dx_3 dz_3 + \epsilon_{z_3y_3} dz_3 dy_3)$$

Using the fact that the strain tensor is symmetric and neglecting any strain component in the plane of the blade cross section (x_3-y_3) because of the blade slenderness, the above equation reduces to

$$2[dx_3 dx_3 dz_3][\epsilon_{ij}]\begin{pmatrix} dx_3 \\ dx_3 \\ dz_3 \end{pmatrix} = 4\epsilon_{z_3x_3} dx_3 dz_3 + 4\epsilon_{z_3y_3} dy_3 dz_3 + 2\epsilon_{z_3z_3} {dz_3}^2 \qquad (3.20)$$

By simplifying the left hand side of eq. (3.19)

$$\bar{dr_1}.\bar{dr_1} - \bar{dr_0}.\bar{dr_0} = \{\left(dx_3 - y_3 k_{z_{B6}} ds_1\right)^2 + \left(dy_3 + x_3 k_{z_{B6}} ds_1\right)^2 + \left(1 - x_3 k_{y_{B6}} +$$

$$y_3 k_{x_{B6}}\right)^2 ds_1^2\} - \{\left(dx_3 - y_3 k_{z_{B3}} ds\right)^2 + \left(dy_3 + x_3 k_{z_{B3}} ds\right)^2 + (1 - x_3 k_{y_{B3}} + y_3 k_{x_{B3}})^2 ds^2\}$$

(3.21)

The relation between ds_1 and ds can be expressed as [10]

$$ds_1 = (1 + 2\,\epsilon_e)^{0.5} ds \qquad (3.22)$$

where ϵ_e is the extensional component of the Green's strain tensor

Substituting eq. (3.22) in to (3.21) and expanding leads to

$$\bar{dr_1}.\bar{dr_1} - \bar{dr_0}.\bar{dr_0} = -ds^2 + ds^2(1 + 2\epsilon_e) + 2ds^2 k_{y_{B3}} x_3 - 2ds^2(1 + 2\epsilon_e) k_{y_{B6}} x_3 -$$

$$2ds dy_3 k_{z_{B3}} x_3 + 2ds(1 + 2\epsilon_e) dy_3 k_{z_{B6}} x_3 - ds^2 k_{y_{B3}}^2 x_3^2 + ds^2(1 + 2\epsilon_e) k_{y_{B6}}^2 x_3^2 - ds^2 k_{z_{B3}}^2 x_3^2 +$$

$$ds^2(1 + 2\epsilon_e) k_{z_{B6}}^2 x_3^2 - 2ds^2 k_{x_{B3}} y_3 + 2ds^2(1 + 2\epsilon_e) k_{x_{B6}} y_3 + 2ds dx_3 k_{z_{B3}} y_3 - 2ds(1 +$$

$$2\epsilon_e) dx_3 k_{z_{B6}} y_3 + 2ds^2 k_{x_{B3}} k_{y_{B3}} x_3 y_3 - 2ds^2(1 + 2\epsilon_e) k_{x_{B6}} k_{y_{B6}} x_3 y_3 - ds^2 k_{x_{B3}}^2 y_3^2 + ds^2(1 +$$

$$2\epsilon_e) k_{x_{B6}}^2 y_3^2 - ds^2 k_{z_{B3}}^2 y_3^2 + ds^2(1 + 2\epsilon_e) k_{z_{B6}}^2 y_3^2$$

Assuming that the extensional strain component ϵ_e is negligible compared to unity, we have

$$\bar{dr_1}.\bar{dr_1} - \bar{dr_0}.\bar{dr_0} = 2ds^2\epsilon_e + 2ds^2k_{y_{B3}}x_3 - 2ds^2k_{y_{B6}}x_3 - 2dsdy_3k_{z_{B3}}x_3 + 2dsdy_3k_{z_{B6}}x_3 - ds^2k_{y_{B3}}^2x_3^2 + ds^2k_{y_{B6}}^2x_3^2 - ds^2k_{z_{B3}}^2x_3^2 + ds^2k_{z_{B6}}^2x_3^2 - 2ds^2k_{x_{B3}}y_3 + 2ds^2k_{x_{B6}}y_3 + 2dsdx_3k_{z_{B3}}y_3 - 2dsdx_3k_{z_{B6}}y_3 + 2ds^2k_{x_{B3}}k_{y_{B3}}x_3y_3 - 2ds^2k_{x_{B6}}k_{y_{B6}}x_3y_3 - ds^2k_{x_{B3}}^2y_3^2 + ds^2k_{x_{B6}}^2y_3^2 - ds^2k_{z_{B3}}^2y_3^2 + ds^2k_{z_{B6}}^2y_3^2 \quad (3.23)$$

Simplifying eq. (3.23) considering ($dz_3 = ds$) along the blade elastic axis

$$\bar{dr_1}.\bar{dr_1} - \bar{dr_0}.\bar{dr_0} = 2(\epsilon_e + x_3(k_{y_{B3}} - k_{y_{B6}}) - y_3(k_{x_{B3}} - k_{x_{B6}}) + x_3y_3(k_{x_{B3}}k_{y_{B3}} - k_{x_{B6}}k_{y_{B6}}) - \frac{y_3^2}{2}(k_{x_{B3}}^2 - k_{x_{B6}}^2) + \frac{x_3^2}{2}(k_{y_{B6}}^2 - k_{y_{B3}}^2) + \frac{(x_3^2+y_3^2)}{2}(k_{z_{B6}}^2 - k_{z_{B3}}^2))dz_3{}^2 - 2x_3(k_{z_{B3}} - k_{z_{B6}})dz_3dy_3 + 2y_3(k_{z_{B3}} - k_{z_{B6}})dz_3dx_3 \quad (3.24)$$

Comparing the right hand side in eq. (3.20) to the left hand side in eq. (3.24) we find

$$\epsilon_{z_3z_3} = \epsilon_e + x_3(k_{y_{B3}} - k_{y_{B6}}) - y_3(k_{x_{B3}} - k_{x_{B6}}) + x_3y_3(k_{x_{B3}}k_{y_{B3}} - k_{x_{B6}}k_{y_{B6}}) - \frac{y_3^2}{2}(k_{x_{B3}}^2 - k_{x_{B6}}^2) + \frac{x_3^2}{2}(k_{y_{B6}}^2 - k_{y_{B3}}^2) + \frac{(x_3^2+y_3^2)}{2}(k_{z_{B6}}^2 - k_{z_{B3}}^2) \quad (3.25)$$

$$\epsilon_{z_3x_3} = \frac{y_3}{2}(k_{z_{B3}} - k_{z_{B6}}) \quad (3.26)$$

$$\epsilon_{z_3y_3} = \frac{x_3}{2}(k_{z_{B3}} - k_{z_{B6}}) \quad (3.27)$$

For calculating the blade strain energy we need to get the strains in equations (3.25), (3.26), and (3.27) in terms of the elastic deformations (*u, v,* and *w*) and the twisting deformation ϕ, where *u, v,* and *w* are deformations in x_3, y_3, and z_3 directions respectively. As in Ref. [10] appendix A

$$\epsilon_e = \alpha_z + \frac{1}{2}(\alpha_x^2 + \alpha_y^2) \quad (3.28)$$

$$k_{x_{B6}} = k_{x_{B3}} - \alpha_x k_{z_{B3}} - \alpha_y{}' - \frac{1}{2}k_{x_{B3}}\alpha_x^2 - \frac{1}{2}k_{x_{B3}}\phi^2 + \phi\alpha_x{}' - \phi\alpha_y k_{z_{B3}} + \phi k_{y_{B3}}$$

$$k_{y_{B6}} = k_{y_{B3}} - \alpha_y k_{z_{B3}} + \alpha_x{}' - \frac{1}{2}k_{y_{B3}}(\alpha_y^2 + \phi^2) + \phi\alpha_y{}' + \phi\alpha_x k_{z_{B3}} - \phi k_{x_{B3}} - k_{x_{B3}}\alpha_x\alpha_y$$

(3.29)

$$k_{z_{B6}} = \alpha_x k_{x_{B3}} + \alpha_y k_{y_{B3}} + k_{z_{B3}} - \frac{1}{2}k_{z_{B3}}(\alpha_y^2 + \alpha_x^2) + \phi' + \alpha_x{}'\alpha_y$$

For case of zero section pitch angle [10]

$$k_{x_{B3}} = 0$$

$$k_{y_{B3}} = -\theta'$$

$$k_{z_{B3}} = 0 \qquad (3.30)$$

$$\alpha_x = u' - w\theta'$$

$$\alpha_y = v'$$

$$\alpha_z = w' + u\theta'$$

Substituting equations (3.28), (3.29), and (3.30) in to equations (3.25), (3.26), (3.27) we get

$$\epsilon_{z_3z_3} = \frac{(v')^2}{2} + w' + u\theta' + \frac{1}{2}(u' - w\theta')^2 + y_3(-\phi\theta' + \phi(u'' - w'\theta' - w\theta'') - v'') -$$

$$x_3(\frac{\theta'}{2}(\phi^2 + (v')^2) + (u'' - w'\theta' - w\theta'') + \phi v'') + x_3^2(-\frac{1}{2}\phi^2(\theta')^2 - \theta'(u'' - w'\theta' - w\theta'') +$$

$$\frac{1}{2}((u'' - w'\theta' - w\theta''))^2 - \phi\theta' v'') + x_3y_3(-\phi(\theta')^2 + 2\phi\theta'(u'' - w'\theta' - w\theta'') - \theta' v'' +$$

$$(u'' - w'\theta' - w\theta'')v'') + y_3^2(\frac{1}{2}\phi^2(\theta')^2 + \frac{1}{2}(v')^2(\theta')^2 + \phi\theta' v'' + \frac{(v'')^2}{2}) + \frac{(x_3^2+y_3^2)}{2}((\phi')^2 -$$

$$v'\theta'\phi') \qquad (3.31)$$

$$\epsilon_{z_3x_3} = -\frac{1}{2}y_3(-v'\theta' + \phi' + v'(u'' - w'\theta' - w\theta'')) \qquad (3.32)$$

$$\epsilon_{z_3y_3} = \frac{1}{2}x_3(-v'\theta' + \phi' + v'(u'' - w'\theta' - w\theta'')) \qquad (3.33)$$

Now substituting equations (3.31), (3.32), and (3.33) in to equation (3.5), we can get the strain energy as a function of *u, v, w,* and ϕ and their derivatives

$$SE = \frac{1}{2}\int_0^S \int_0^{Y_3} \int_0^{X_3} \{E\left[\left(\frac{(v')^2}{2} + w' + u\theta' + \frac{1}{2}(u' - w\theta')^2 + y_3(-\phi\theta' + \phi(u'' - w'\theta' - w\theta'') - v'') - x_3\left(\frac{\theta'}{2}(\phi^2 + (v')^2) + (u'' - w'\theta' - w\theta'') + \phi v''\right) + x_3^2\left(-\frac{1}{2}\phi^2(\theta')^2 - \theta'(u'' - w'\theta' - w\theta'') + \frac{1}{2}\left((u'' - w'\theta' - w\theta'')\right)^2 - \phi\theta' v''\right) + x_3 y_3(-\phi(\theta')^2 + 2\phi\theta'(u'' - w'\theta' - w\theta'') - \theta' v'' + (u'' - w'\theta' - w\theta'')v'') + y_3^2\left(\frac{1}{2}\phi^2(\theta')^2 + \frac{1}{2}(v')^2(\theta')^2 + \phi\theta' v'' + \frac{(v'')^2}{2}\right) + \frac{(x_3^2 + y_3^2)}{2}((\phi')^2 - v'\theta'\phi')\right)^2\right] + 4G\left[\left(-\frac{1}{2}y_3\left(-v'\theta' + \phi' + v'(u'' - w'\theta' - w\theta'')\right)\right)^2 + \left(\frac{1}{2}x_3\left(-v'\theta' + \phi' + v'(u'' - w'\theta' - w\theta'')\right)\right)^2\right]\} dx_3\, dy_3\, dz_3 \qquad (3.34)$$

Because we seeking linear system of equations from Lagrange's equation we will keep quadratic terms only so we can simplify eq. (3.34) as follows:

$$SE = \frac{1}{2}\int_0^S \int_0^{Y_3} \int_0^{X_3} \{E[(w' + u\theta' + y_3(-\phi\theta' - v'') - x_3(u'' - w'\theta' - w\theta'') + x_3^2(-\theta'(u'' - w'\theta' - w\theta'')) + x_3 y_3(-\phi(\theta')^2 - \theta' v''))^2] + 4G[\left(-\frac{1}{2}y_3(-v'\theta' + \phi')\right)^2 + \left(\frac{1}{2}x_3(-v'\theta' + \phi')\right)^2]\} dx_3\, dy_3\, dz_3 \qquad (3.35)$$

where

u, v, w, ϕ, and their derivatives represent *u(s,t) , v(s,t) , w(s,t) , ϕ(s,t)* and their derivatives.

Assuming that the blade cross section shown in figure 3.2 is symmetric about Y_{B3}-axis, the cross sectional properties resulting from expanding eq. (3.35) are defined as follows

1. The blade cross section area $\quad A = \int\int dx_3\, dy_3$

2. $Ae_A = \int\int y_3\, dx_3\, dy_3$ {e_A is the chord-wise offset of area centeroid of cross section from elastic axis (has a positive value when measured in front of elastic axis and vice versa)}
3. Edge-wise second moment of area of blade cross section $I_{x_3x_3} = \int\int {y_3}^2\, dx_3\, dy_3$
4. Flat-wise second moment of area of blade cross section $I_{y_3y_3} = \int\int {x_3}^2\, dx_3\, dy_3$
5. Polar second moment of area $J = \int\int ({y_3}^2 + {x_3}^2)\, dx_3\, dy_3$
6. $\int\int x_3\, dx_3\, dy_3 = 0$
7. $\int\int x_3 y_3\, dx_3\, dy_3 = 0$
8. $\int\int x_3({x_3}^2 + {y_3}^2)\, dx_3\, dy_3 = 0$
9. $\int\int y_3 {x_3}^3\, dx_3\, dy_3 = 0$
10. $\int\int x_3 {y_3}^3\, dx_3\, dy_3 = 0$
11. $\int\int x_3 {y_3}^2\, dx_3\, dy_3 = 0$
12. $P_1 = \int\int {x_3}^4\, dx_3\, dy_3$
13. $P_2 = \int\int x_3^2 y_3\, dx_3\, dy_3$
14. $P_3 = \int\int x_3^2 y_3^2\, dx_3\, dy_3$

Substituting the above blade cross sectional properties and expanding we get

$$SE = \frac{1}{2}\int_0^S \{E[A((w')^2 + 2uw'\theta' + u^2(\theta')^2) - 2Ae_A(\phi w'\theta' + u\phi(\theta')^2 + w'v'' + u\theta'v'') +$$

$$I_{x_3x_3}(\phi^2(\theta')^2 + 2\phi\theta'v'' + (v'')^2) + P_3(\phi^2(\theta')^4 + 2\phi(\theta')^3v'' + (\theta')^2(v'')^2) +$$

$$4P_2(-\phi w'(\theta')^3 + \phi(\theta')^2u'' - w'(\theta')^2v'' + \theta'u''v'' - w\phi(\theta')^2\theta'' - w\theta'v''\theta'') +$$

$$I_{y_3y_3}(3(w')^2(\theta')^2 + 2uw'(\theta')^3 - 4w'\theta'u'' - 2u(\theta')^2u'' + (u'')^2 + 4ww'\theta'\theta'' +$$

$$2uw(\theta')^2\theta'' - 2wu''\theta'' + w^2(\theta'')^2) + P_1((w')^2(\theta')^4 - 2w'(\theta')^3u'' + (\theta')^2(u'')^2 +$$

$$2ww'(\theta')^3\theta'' - 2w(\theta')^2u''\theta'' + w^2(\theta')^2(\theta'')^2)] + GJ[((v')^2(\theta')^2 - 2v'\theta'\phi' + (\phi')^2)]\}\, ds$$

(3.36)

3.3 Kinetic energy

The kinetic energy of the blade in terms of $\bar{r}_1$ can be given by

$$T = \frac{1}{2}\int_0^S \int_0^{Y_3} \int_0^{X_3} \rho\left(\frac{d\bar{r}_1}{dt}.\frac{d\bar{r}_1}{dt}\right) dx_3\, dy_3\, dz_3) \qquad (3.37)$$

In eq. (3.36)

$$\frac{d\bar{r}_1}{dt} = \dot{r}_1 + \bar{\omega} \times \bar{r}_1 \qquad (3.38)$$

With reference to figure 3.3

$\bar{\omega}$ is the angular velocity of the B3-system.

$\bar{r}_1$ is the position vector of an arbitrary mass point on the blade.

Note: $\bar{\omega}$ and $\bar{r}_1$ are not shown in figure 3.3. Then

$$\bar{r}_1 = \bar{R} + \Delta\bar{R} + x_3\bar{e}_{x_{B6}} + y_3\bar{e}_{y_{B6}} \qquad (3.39)$$

$$\bar{R} = x_0\bar{e}_{x_I} + z_0\bar{e}_{z_I}$$

For a nonrotating blade

$$\bar{R} = x_0\bar{e}_{x_R} + z_0\bar{e}_{z_R}$$

Because the *R*-system and *B1*-system are parallel we can express $\bar{R}$ as

$$\bar{R} = x_0\bar{e}_{x_{B1}} + z_0\bar{e}_{z_{B1}}$$

The coordinate transformation between the *B1* and *B2* coordinate systems is

$$\begin{pmatrix} \bar{e}_{x_{B1}} \\ \bar{e}_{y_{B1}} \\ \bar{e}_{z_{B1}} \end{pmatrix} = \begin{bmatrix} cos\theta & 0 & -sin\theta \\ 0 & 1 & 0 \\ sin\theta & 0 & cos\theta \end{bmatrix} \begin{pmatrix} \bar{e}_{x_{B2}} \\ \bar{e}_{y_{B2}} \\ \bar{e}_{z_{B2}} \end{pmatrix} \qquad (3.40)$$

Using eq. (3.40)

$$\bar{R} = (x_0 cos\theta + z_0 sin\theta)\bar{e}_{x_{B2}} + (z_0 cos\theta - x_0 sin\theta)\bar{e}_{z_{B2}}$$

For zero section pitch angle *B2* and *B3* are the same so:

$$\bar{R} = (x_0 cos\theta + z_0 sin\theta)\bar{e}_{x_{B3}} + (z_0 cos\theta - x_0 sin\theta)\bar{e}_{z_{B3}} \qquad (3.41)$$

With reference to figure 3.3

Note: *u, v, w* are not shown in figure 3.3

$$\Delta\bar{R} = u\bar{e}_{x_{B3}} + v\bar{e}_{y_{B3}} + w\bar{e}_{z_{B3}} \qquad (3.42)$$

The rotational transformation matrix [T] from *B3* to *B6* coordinates can be formulated by Eulerian-type angles [8] β, θ, and ζ, which can be defined as follows:

1. β is the positive rotation angle about y_{B_3}- axis which converts $x_{B_3}y_{B_3}z_{B_3}$ to $x_{B_4}y_{B_4}z_{B_4}$ (not shown)
2. ζ is the positive rotation angle about the negative x_{B_4}- axis which converts $x_{B_4}y_{B_4}z_{B_4}$ to $x_{B_5}y_{B_5}z_{B_5}$(not shown)
3. σ is the positive rotation about z_{B_5} - axis which converts $x_{B_5}y_{B_5}z_{B_5}$ to $x_{B_6}y_{B_6}z_{B_6}$.

Applying these three rotations we get [T] as follows:

$$[T] = \begin{bmatrix} cos(\beta)cos(\sigma) - sin(\sigma)sin(\zeta)sin(\beta) & cos(\zeta)sin(\sigma) & -cos(\sigma)sin(\beta) - sin(\sigma)sin(\zeta)cos(\beta) \\ -cos(\beta)sin(\sigma) - cos(\sigma)sin(\zeta)sin(\beta) & cos(\zeta)cos(\sigma) & sin(\beta)sin(\sigma) - cos(\sigma)sin(\zeta)cos(\beta) \\ cos(\zeta)sin(\beta) & sin(\zeta) & cos(\beta)cos(\zeta) \end{bmatrix}$$

(3.43)

Rewriting [T] matrix as a function of strain components *u, v, w*, and ϕ we get [10]

$$[T] = \begin{bmatrix} 1 - \frac{\phi^2}{2} - \frac{1}{2}(u' - \theta' w)^2 & \phi & -(u' - \theta' w) - \phi v' \\ -\phi - (u' - \theta' w)v' & 1 - \frac{\phi^2}{2} - \frac{v'^2}{2} & \phi(u' - \theta' w) - v' \\ (u' - \theta' w) & v' & 1 - \frac{1}{2}[(u' - \theta' w)^2 - v'^2] \end{bmatrix} \qquad (3.44)$$

The transformation from unit vectors in the *B3*- coordinate system to unit vectors in B6- coordinate system can be written as

$$\begin{pmatrix} \bar{e}_{x_{B6}} \\ \bar{e}_{y_{B6}} \\ \bar{e}_{z_{B6}} \end{pmatrix} = [T] \begin{pmatrix} \bar{e}_{x_{B3}} \\ \bar{e}_{y_{B3}} \\ \bar{e}_{z_{B3}} \end{pmatrix} \tag{3.45}$$

Using eq. (3.45) with eq. (3.44)

$$\bar{e}_{x_{B6}} = (1 - \frac{\phi^2}{2} - \frac{{\alpha_x}^2}{2})\bar{e}_{x_{B3}} + \phi\bar{e}_{y_{B3}} + (-\alpha_x - \phi\alpha_y)\bar{e}_{z_{B3}}$$

$$\bar{e}_{y_{B6}} = (-\phi - \alpha_x\alpha_y)\bar{e}_{x_{B3}} + (1 - \frac{\phi^2}{2} - \frac{{\alpha_y}^2}{2})\bar{e}_{y_{B3}} + (\phi\alpha_x - \alpha_y)\bar{e}_{z_{B3}} \tag{3.46}$$

Substituting equations (3.41), (3.42), and (3.46) in to equation 3.39 we get

$$\bar{r}_1 = \left(x_0 cos\theta + z_0 sin\theta + u + x_3\left(1 - \frac{\phi^2}{2} - \frac{{\alpha_x}^2}{2}\right) - y_3\left(\phi + \alpha_x\alpha_y\right)\right)\bar{e}_{x_{B3}} + (v + x_3\phi + y_3(1 -$$

$$\frac{\phi^2}{2} - \frac{{\alpha_y}^2}{2}))\bar{e}_{y_{B3}} + (z_0 cos\theta - x_0 sin\theta + w - x_3(\alpha_x + \phi\alpha_y) + y_3(\phi\alpha_x - \alpha_y))\bar{e}_{z_{B3}} \tag{3.47}$$

Substituting for α_x and α_y from eq. (3.30) in to eq. (3.47)

$$\bar{r}_1 = \left[x_0 cos\theta + z_0 sin\theta + u + x_3\left(1 - \frac{\phi^2}{2} - \frac{\left((u')^2 - 2wu'\theta' + w^2(\theta')^2\right)}{2}\right) - y_3\big(\phi + (v'u' -\right.$$

$$\left.v'w\theta')\big)\right]\bar{e}_{x_{B3}} + \left[v + x_3\phi + y_3\left(1 - \frac{\phi^2}{2} - \frac{{v'}^2}{2}\right)\right]\bar{e}_{y_{B3}} + [z_0 cos\theta - x_0 sin\theta + w - x_3(u' -$$

$$w\theta' + \phi v') + y_3(\phi u' - \phi w\theta' - v')]\bar{e}_{z_{B3}} \tag{3.48}$$

From eq. (3.48)

$$\dot{\bar{r}}_1 = \left[\dot{u} + x_3\big(-\phi\dot{\phi} - u'\dot{u'} - \theta'\big(\dot{w}u' + w\dot{u'}\big) + w\dot{w}(\theta')^2\big) - y_3\left(\dot{\phi} + \dot{v'}u' + v'\dot{u'} -\right.\right.$$

$$\left.\left.\theta'\big(\dot{v'}w + v'\dot{w}\big)\right)\right]\bar{e}_{x_{B3}} + \left[\dot{v} + x_3\dot{\phi} + y_3\big(-\phi\dot{\phi} - v'\dot{v'}\big)\right]\bar{e}_{y_{B3}} + [\dot{w} - x_3\big(\dot{u'} - \dot{w}\theta' + \dot{\phi}v' +$$

$$\phi\dot{v'}\big) + y_3\big(\dot{\phi}u' + \phi\dot{u'} - \theta'\big(\dot{\phi}w + \phi\dot{w}\big) - \dot{v'}\big)]\bar{e}_{z_{B3}} \tag{3.49}$$

The angular velocity of the *B3*-coordinate system can be expressed as

$$\bar{\omega} = \Omega \bar{e}_{z_I} = \Omega \bar{e}_{z_R} = \Omega \bar{e}_{z_{B1}} \qquad (3.50)$$

Substituting for $\bar{e}_{z_{B1}}$ from equation (3.40) and for case of zero section pitch angle

$$\bar{\omega} = \Omega sin\theta \bar{e}_{x_{B3}} + \Omega cos\theta \bar{e}_{z_{B3}} \qquad (3.51)$$

so

$$\bar{\omega} \times \bar{r}_1 = -\left[\left(v + x_3\phi + y_3\left(1 - \frac{\phi^2}{2} - \frac{v'^2}{2}\right)\right)\Omega cos\theta\right]\bar{e}_{x_{B3}} - \Big[\big(z_0 cos\theta - x_0 sin\theta + w -$$

$$x_3(u' - w\theta' + \phi v') + y_3(\phi u' - \phi w\theta' - v')\big)\Omega sin\theta - \Bigg(x_0 cos\theta + z_0 sin\theta + u +$$

$$x_3\left(1 - \frac{\phi^2}{2} - \frac{\left((u')^2 - 2wu'\theta' + w^2(\theta')^2\right)}{2}\right) - y_3\big(\phi + (v'u' - v'w\theta')\big)\Bigg)\Omega cos\theta\Bigg]\bar{e}_{y_{B3}} + [\Bigg(v + x_3\phi +$$

$$y_3\left(1 - \frac{\phi^2}{2} - \frac{v'^2}{2}\right)\Bigg)\Omega sin\theta]\bar{e}_{z_{B3}} \qquad (3.52)$$

Substituting equations (3.49) and (3.52) in to equation 3.38 we find

$$\frac{d\bar{r}_1}{dt} = \Bigg[\Big(\dot{u} + x_3\big(-\phi\dot{\phi} - u'\dot{u}' + \theta'\big(\dot{w}u' + w\dot{u}'\big) - w\dot{w}(\theta')^2\big) - y_3\Big(\dot{\phi} + \dot{v}'u' + v'\dot{u}' -$$

$$\theta'\big(\dot{v}'w + v'\dot{w}\big)\Big)\Big) - \Bigg(\Bigg(v + x_3\phi + y_3\left(1 - \frac{\phi^2}{2} - \frac{v'^2}{2}\right)\Bigg)\Omega cos\theta\Bigg)\Bigg]\bar{e}_{x_{B3}} + \Bigg[\Big(\dot{v} + x_3\dot{\phi} +$$

$$y_3\big(-\phi\dot{\phi} - v'\dot{v}'\big)\Big) - \Bigg(\big(z_0 cos\theta - x_0 sin\theta + w - x_3(u' - w\theta' + \phi v') + y_3(\phi u' - \phi w\theta' -$$

$$v')\big)\Omega sin\theta + \Bigg(x_0 cos\theta + z_0 sin\theta + u + x_3\left(1 - \frac{\phi^2}{2} - \frac{\left((u')^2 - 2wu'\theta' + w^2(\theta')^2\right)}{2}\right) - y_3\big(\phi +$$

$$(v'u' - v'w\theta'))\Big)\Omega cos\theta\Big)\Big]\bar{e}_{y_{B3}} + [\Big(\dot{w} - x_3\big(\dot{u'} - \dot{w}\theta' + \dot{\phi}v' + \phi\dot{v'}\big) + y_3\big(\dot{\phi}u' + \phi\dot{u'} -$$

$$\theta'\big(\dot{\phi}w + \phi\dot{w}\big) - \dot{v'}\big)\Big) + \Bigg(\Bigg(v + x_3\phi + y_3\left(1 - \frac{\phi^2}{2} - \frac{v'^2}{2}\right)\Bigg)\Omega sin\theta\Bigg)]\bar{e}_{z_{B3}} \qquad (3.53)$$

Now we can get an expression for the kinetic energy as a function of *u, v, w,* and ϕ and the inertial coordinates of the elastic axis by substituting eq. (3.53) into eq. (3. 37) to get

$$T = \frac{1}{2}\rho \int_0^S \int_0^{Y_3} \int_0^{X_3} \{\Big[\Big(\dot{u} + x_3\big(-\phi\dot{\phi} - u'\dot{u'} - \theta'\big(\dot{w}u' + w\dot{u'}\big) + w\dot{w}(\theta')^2\big) - y_3\Big(\dot{\phi} +$$

$$\dot{v'}u' + v'\dot{u'} - \theta'\big(\dot{v'}w + v'\dot{w}\big)\Big)\Big) - \Bigg(\Bigg(v + x_3\phi + y_3\left(1 - \frac{\phi^2}{2} - \frac{v'^2}{2}\right)\Bigg)\Omega cos\theta\Bigg)\Big]^2 +$$

$$\Big[\Big(\dot{v} + x_3\dot{\phi} + y_3\big(-\phi\dot{\phi} - v'\dot{v'}\big)\Big) - \Bigg(\big(z_0 cos\theta - x_0 sin\theta + w - x_3(u' - w\theta' + \phi v') +$$

$$y_3(\phi u' - \phi w\theta' - v')\big)\Omega sin\theta - \Bigg(x_0 cos\theta + z_0 sin\theta + u + x_3\Bigg(1 - \frac{\phi^2}{2} -$$

$$\frac{\big((u')^2 - 2wu'\theta' + w^2(\theta')^2\big)}{2}\Bigg) - y_3\big(\phi + (v'u' - v'w\theta')\big)\Bigg)\Omega cos\theta\Bigg)\Big]^2 + \Big[\Big(\dot{w} - x_3\big(\dot{u'} - \dot{w}\theta' + \dot{\phi}v' +$$

$$\phi\dot{v'}\big) + y_3\big(\dot{\phi}u' + \phi\dot{u'} - \theta'\big(\dot{\phi}w + \phi\dot{w}\big) - \dot{v'}\big)\Big) + \Bigg(\Bigg(v + x_3\phi + y_3\Bigg(1 - \frac{\phi^2}{2} -$$

$$\frac{v'^2}{2}\Bigg)\Bigg)\Omega sin\theta\Bigg)\Big]^2\} dx_3\, dy_3\, dz_3 \qquad (3.54)$$

Simplifying eq. (3.54) by keeping quadratic powers and neglecting any higher order terms (linearize) and using the following blade cross sectional properties

1. The blade mass per unit length $m = \int\int \rho \, \mathrm{d}x_3 \, \mathrm{d}y_3$
2. $\mathrm{me} = \int\int \rho y_3 \, \mathrm{d}x_3 \, \mathrm{d}y_3$ {e is the chord-wise offset of mass centeroid of cross section from elastic axis (has a positive value when measured in front of elastic axis and vice versa)}
3. Mass moment of inertia about Y_3-axis $I_{my_3} = \int\int \rho x_3^2 \, \mathrm{d}x_3 \, \mathrm{d}y_3$
4. Mass moment of inertia about X_3-axis $I_{mx_3} = \int\int \rho y_3^2 \, \mathrm{d}x_3 \, \mathrm{d}y_3$
5. $\int\int \rho x_3 \, \mathrm{d}x_3 \, \mathrm{d}y_3 = 0$
6. $\int\int \rho x_3 y_3 \, \mathrm{d}x_3 \, \mathrm{d}y_3 = 0$

Eq. 3.53 can be rewritten as

$$T = \frac{1}{2}\int_0^S \{m(\dot{u}^2 + \dot{v}^2 + \dot{w}^2) + \mathrm{me}(-2\dot{u}\dot{\phi} - 2\dot{w}\dot{v}') + I_{m_{x_3}}(\dot{\phi}^2 + \dot{v}'^2) + I_{m_{y_3}}(\dot{\phi}^2 + \dot{u}'^2 - 2\dot{w}\dot{u}'\theta' + \dot{w}^2(\theta')^2)\} \, \mathrm{d}s \qquad (3.55)$$

Note that in eq. (55); $\dot{(\,)} = \frac{\partial}{\partial \mathrm{t}}$

3.4 Discretization of energy expressions for modal analysis

In this section we will use modal functions of a uniform clamped-clamped beam as an approximation for the assumed modal functions of the clamped-clamped Darrieus wind turbine blade with troposkein shape.

For simplicity we will consider the Sandia blade to get expressions for mass and stiffness matrices. The modal functions of a clamped-clamped beam [21] under the same deformation conditions of the blade are:

1. flat-wise bending

$$\psi_{u_j}(s) = \sum_{j=1}^{n}\{ cosh[\frac{\lambda_j s}{l}] - \frac{(cosh[\lambda_j]-cos[\lambda_j])sinh\left[\frac{\lambda_j s}{l}\right]}{sinh[\lambda_j]-sin[\lambda_j]} - cos[\frac{\lambda_j s}{l}] + \frac{(cosh[\lambda_j]-cos[\lambda_j])sin\left[\frac{\lambda_j s}{l}\right]}{sinh[\lambda_j]-sin[\lambda_j]}\}$$

(3.56)

2. Edge-wise bending

$$\psi_{v_j}(s) = \sum_{j=1}^{n}\{ cosh[\frac{\lambda_j s}{l}] - \frac{(cosh[\lambda_j]-cos[\lambda_j])sinh\left[\frac{\lambda_j s}{l}\right]}{sinh[\lambda_j]-sin[\lambda_j]} - cos[\frac{\lambda_j s}{l}] + \frac{(cosh[\lambda_j]-cos[\lambda_j])sin\left[\frac{\lambda_j s}{l}\right]}{sinh[\lambda_j]-sin[\lambda_j]}\}$$

(3.57)

3. Extension

$$\psi_{w_j}(s) = \sum_{j=1}^{n}\{ sin[\frac{j\pi s}{l}]\} \quad (3.58)$$

4. Torsion

$$\psi_{\phi_j}(s) = \sum_{j=1}^{n}\{ sin[\frac{j\pi s}{l}]\} \quad (3.59)$$

We can express u, v, w, and ϕ as functions of the assumed modal functions ψ(s) and assumed modal coordinates q (t) as follows

$$u_j(s,t) = \sum_{j=1}^{n}\{ q_{u_j}(t)\, \psi_{u_j}(s)\} \quad (3.60)$$

$$v_j(s,t) = \sum_{j=1}^{n}\{ q_{v_j}(t)\, \psi_{v_j}(s)\} \quad (3.61)$$

$$w_j(s,t) = \sum_{j=1}^{n}\{ q_{w_j}(t)\, \psi_{w_j}(s)\} \quad (3.62)$$

$$\phi_j(s,t) = \sum_{j=1}^{n}\{ q_{\phi_j}(t)\, \psi_{\phi_j}(s)\} \quad (3.63)$$

Substituting eqns. (3.56) - (3.59) in eqns. (3.60)-(3.63) we get

$$u_j(s,t) = \sum_{j=1}^{n}\{ q_{u_j}(t)(cosh[\frac{\lambda_j s}{l}] - \frac{(cosh[\lambda_j]-cos[\lambda_j])sinh\left[\frac{\lambda_j s}{l}\right]}{sinh[\lambda_j]-Sin[\lambda_j]} - cos[\frac{\lambda_j s}{l}] +$$

$$\frac{(cosh[\lambda_j]-cos[\lambda_j])sin\left[\frac{\lambda_j s}{l}\right]}{sinh[\lambda_j]-sin[\lambda_j]}\} \quad (3.64)$$

$$v_j(s,t) = \sum_{j=1}^{n}\{ q_{v_j}(t)(cosh[\frac{\lambda_j s}{l}] - \frac{(cosh[\lambda_j]-cos[\lambda_j])sinh\left[\frac{\lambda_j s}{l}\right]}{sinh[\lambda_j]-sin[\lambda_j]} - cos[\frac{\lambda_j s}{l}] + \frac{(cosh[\lambda_j]-cos[\lambda_j])sin\left[\frac{\lambda_j s}{l}\right]}{sinh[\lambda_j]-sin[\lambda_j]}\}$$

(3.65)

$$w_j(s,t) = \sum_{j=1}^{n}\{ q_{w_j}(t)sin[\frac{j\pi s}{l}]\} \qquad (3.65)$$

$$\phi_j(s,t) = \sum_{j=1}^{n}\{ q_{\phi_j}(t)sin[\frac{j\pi s}{l}]\} \qquad (3.66)$$

3.4.1 Derivation of stiffness matrix expressions

Putting equations (3.60)-(3.63) into equation (3.36) we get

$$SE = \sum_{j=1}^{n}\sum_{k=1}^{n} 0.5 \int_0^S \{A[Eu_j u_k(\theta')^2 + Eu_k\theta' w_j' + Eu_j\theta' w_k' + Ew_j' w_k'] +$$

$$P_1[E(\theta')^4 w_j' w_k' + Ew_k(\theta')^3 w_j'\theta'' + Ew_j(\theta')^3 w_k'\theta'' + Ew_j w_k(\theta')^2(\theta'')^2 - E(\theta')^3 w_k' u_j'' -$$

$$Ew_k(\theta')^2\theta'' u_j'' - E(\theta')^3 w_j' u_k'' - Ew_j(\theta')^2\theta'' u_k'' + E(\theta')^2 u_j'' u_k''] + Ae_A[-Eu_k\phi_j(\theta')^2 -$$

$$Eu_j\phi_k(\theta')^2 - E\phi_k\theta' w_j' - E\phi_j\theta' w_k' - Eu_k\theta' v_j'' - Ew_k' v_j'' - Eu_j\theta' v_k'' - Ew_j' v_k''] +$$

$$I_{x_3x_3}[E\phi_j\phi_k(\theta')^2 + G(\theta')^2 v_j' v_k' - G\theta' v_k'\phi_j' - G\theta' v_j'\phi_k' + G\phi_j'\phi_k' + E\phi_k\theta' v_j'' +$$

$$E\phi_j\theta' v_k'' + Ev_j'' v_k''] + p_3[E\phi_j\phi_k(\theta')^4 + E\phi_k(\theta')^3 v_j'' + E\phi_j(\theta')^3 v_k'' + E(\theta')^2 v_j'' v_k''] +$$

$$I_{y_3y_3}[G(\theta')^2 v_j' v_k' + Eu_k(\theta')^3 w_j' + Eu_j(\theta')^3 w_k' + 3E(\theta')^2 w_j' w_k' - G\theta' v_k'\phi_j' -$$

$$G\theta' v_j'\phi_k' + G\phi_j'\phi_k' + Eu_k w_j(\theta')^2\theta'' + Eu_j w_k(\theta')^2\theta'' + 2Ew_k\theta' w_j'\theta'' + 2Ew_j\theta' w_k'\theta'' +$$

$$Ew_j w_k(\theta'')^2 - Eu_k(\theta')^2 u_j'' - 2E\theta' w_k' u_j'' - Ew_k\theta'' u_j'' - Eu_j(\theta')^2 u_k'' - 2E\theta' w_j' u_k'' -$$

$$Ew_j\theta'' u_k'' + Eu_j'' u_k''] + P_2[-2E\phi_k(\theta')^3 w_j' - 2E\phi_j(\theta')^3 w_k' - 2Ew_k\phi_j(\theta')^2\theta'' -$$

$$2Ew_j\phi_k(\theta')^2\theta'' + 2E\phi_k(\theta')^2 u_j'' + 2E\phi_j(\theta')^2 u_k'' - 2E(\theta')^2 w_k' v_j'' - 2Ew_k\theta'\theta'' v_j'' +$$

$$2E\theta' u_k'' v_j'' - 2E(\theta')^2 w_j' v_k'' - 2Ew_j\theta'\theta'' v_k'' + 2E\theta' u_j'' v_k'']\} ds \qquad (3.67)$$

Combining eqns. (3.60-3.63) with eq. (3.67) and simplifying using the blade cross sectional properties, we can express the stiffness matrices equations as follows

1. Flat-wise only

$$K_{jk}^{uu} = \frac{1}{2}E\int_0^S \{A\theta'[s]^2\psi_{u_j}[s]\psi_{u_k}[s] + I_{y_3y_3}(-2\theta'[s]^2\psi_{u_j}[s]\psi_{u_k}''[s] + \psi_{u_j}''[s]\psi_{u_k}''[s]) +$$

$$P_1\theta'[s]^2\psi_{u_j}''[s]\psi_{u_k}''[s]\}\,ds \qquad (3.68)$$

2. Edge-wise only

$$\mathrm{K_{jk}^{vv}} = \int_0^S (\tfrac{1}{2}\mathrm{E}(\mathrm{I_{x_3x_3}}\psi_{\mathrm{v_j}}''[s]\psi_{\mathrm{v_k}}''[s] + \mathrm{P_3}\theta'[s]^2\psi_{\mathrm{v_j}}''[s]\psi_{\mathrm{v_k}}''[s]) + \tfrac{1}{2}\mathrm{G(J)}\theta'[s]^2\psi_{\mathrm{v_j}}'[s]\psi_{\mathrm{v_k}}'[s])\,\mathrm{ds}$$

(3.69)

3. Extension only

$$K_{jk}^{ww} = \frac{1}{2}E\int_0^S (A\psi_{w_j}'[s]\psi_{w_k}'[s] + I_{y_3y_3}(\theta''[s]^2\psi_{w_j}[s]\psi_{w_k}[s] + 4\theta'[s]\theta''[s]\psi_{w_j}[s]\psi_{w_k}'[s] +$$

$$3\theta'[s]^2\psi_{w_j}'[s]\psi_{w_k}'[s]) + P_1(\theta'[s]^2\theta''[s]^2\psi_{w_j}[s]\psi_{w_k}[s] + 2\theta'[s]^3\theta''[s]\psi_{w_j}[s]\psi_{w_k}'[s] +$$

$$\theta'[s]^4\psi_{w_j}'[s]\psi_{w_k}'[s]))\,ds \qquad (3.70)$$

4. Torsion only

$$K_{jk}^{\phi\phi} = \int_0^S (\tfrac{1}{2}E(I_{x_3x_3}\theta'[s]^2\psi_{\phi_j}[s]\psi_{\phi_k}[s] + P_3\theta'[s]^4\psi_{\phi_j}[s]\psi_{\phi_k}[s]) + \tfrac{1}{2}GJ\psi_{\phi_j}'[s]\psi_{\phi_k}'[s])\,ds$$

(3.71)

5. Flat wise-Edge wise

$$K_{jk}^{uv} = \int_0^S \tfrac{1}{2}E1(-2Ae_A\theta'[s]\psi_{u_j}[s]\psi_{v_k}''[s] + 4P_2\theta'[s]\psi_{u_j}''[s]\psi_{v_k}''[s])\,ds \quad (3.72)$$

6. Flat wise – extension

$$K_{jk}^{uw} = \frac{1}{2}E\int_0^S \{A(2\theta'[s]\psi_{u_j}[s]\psi_{w_k}'[s]) + I_{y_3y_3}(2\theta'[s]^2\theta''[s]\psi_{u_j}[s]\psi_{w_k}[s] +$$

$$2\theta'[s]^3\psi_{u_j}[s]\psi_{w_k}'[s] - 2\theta''[s]\psi_{w_k}[s]\psi_{u_j}''[s] - 4\theta'[s]\psi_{w_k}'[s]\psi_{u_j}''[s]) +$$

$P_1(-2\theta'[s]^2\theta''[s]\psi_{w_k}[s]\psi_{u_j}''[s] - 2\theta'[s]^3\psi_{w_k}'[s]\psi_{u_j}''[s])\}\,ds$

(3.73)

7. Flat wise-torsion

$$K_{jk}^{u\phi} = \frac{1}{2}E\int_0^S \{-2Ae_A\theta'[s]^2\psi_{u_j}[s]\psi_{\phi_k}[s] + 4P_2\theta'[s]^2\psi_{\phi_k}[s]\psi_{u_j}''[s]\}\,ds \qquad (3.74)$$

8. Edge wise-extension

$$K_{jk}^{vw} = \frac{1}{2}E\int_0^S \{-2Ae_A\psi_{w_k}'[s]\psi_{v_j}''[s] + P_2(-4\theta'[s]\theta''[s]\psi_{w_k}'[s]\psi_{v_j}''[s] -$$

$$4\theta'[s]^2\psi_{w_k}'[s]\psi_{v_j}''[s])\}\,ds \qquad (3.75)$$

9. Edge wise-torsion

$$K_{jk}^{v\phi} = \int_0^S \{E(I_{x_3x_3}\theta'[s]\psi_{\phi_k}[s]\psi_{v_j}''[s] + P_3\theta'[s]^3\psi_{\phi_k}[s]\psi_{v_j}''[s]) -$$

$$GJ\theta'[s]\psi_{v_j}'[s]\psi_{w_k}'[s]\}\,ds \quad (3.76)$$

10. Extension-torsion

$$K_{jk}^{w\phi} = E\int_0^S \{-Ae_A\theta'[s]\psi_{\phi_k}[s]\psi_{w_j}'[s] + P_2(-2\theta'[s]^2\theta''[s]\psi_{w_j}[s]\psi_{\phi_k}[s] -$$

$$2\theta'[s]^3\psi_{\phi_k}[s]\psi_{w_j}'[s])\}\,ds \qquad (3.77)$$

Note that the stiffness matrix of the blade is symmetric so we have

$$K_{jk}^{uv} = K_{jk}^{vu}$$

$$K_{jk}^{uw} = K_{jk}^{wu}$$

$$K_{jk}^{u\phi} = K_{jk}^{\phi u}$$

$$K_{jk}^{vw} = K_{jk}^{wv} \qquad (3.78)$$

$$K_{jk}^{v\phi} = K_{jk}^{\phi v}$$

$$K_{jk}^{w\phi} = K_{jk}^{\phi w}$$

3.4.2 Derivation of mass matrix expressions

In this section the mass matrix expressions were derived for the nonrotating blade condition (for simplicity Ω = 0). For *u, v, w,* and ϕ as expressed in eqns. (3.60-3.63) we can rewrite eq. (3.55) as

$$T = \frac{1}{2}\rho \sum_{j=1}^{n} \sum_{k=1}^{n} \int_{0}^{S} \int_{0}^{Y_3} \int_{0}^{X_3} \{\psi_{u_j}[s]\psi_{u_k}[s]\dot{q}_{u_j}[t]\dot{q}_{u_k}[t] +$$

$$\psi_{v_j}[s]\psi_{v_k}[s]\dot{q}_{v_j}[t]\dot{q}_{v_k}[t] + \psi_{w_j}[s]\psi_{w_k}[s]\dot{q}_{w_j}[t]\dot{q}_{w_k}[t] + x_3^2\psi_{\phi_j}[s]\psi_{\phi_k}[s]\dot{q}_{\phi_j}[t]\dot{q}_{\phi_k}[t] +$$

$$x_3^2\psi_{u_j}{}'[s]\psi_{u_k}{}'[s]\dot{q}_{u_j}[t]\dot{q}_{u_k}[t] - 2y_3\psi_{u_j}[s]\psi_{\phi_k}[s]\dot{q}_{u_j}[t]\dot{q}_{\phi_k}[t] -$$

$$2y_3\psi_{v_j}{}'[s]\psi_{w_k}[s]\dot{q}_{v_j}[t]\dot{q}_{w_k}[t] + y_3^2\psi_{\phi_j}[s]\psi_{\phi_k}[s]\dot{q}_{\phi_j}[t]\dot{q}_{\phi_k}[t] +$$

$$y_3^2\psi_{v_j}{}'[s]\psi_{v_k}{}'[s]\dot{q}_{v_j}[t]\dot{q}_{v_k}[t] - 2x_3^2\theta'[s]\psi_{u_j}{}'[s]\psi_{w_k}[s]\dot{q}_{u_j}[t]\dot{q}_{w_k}[t] +$$

$$x_3^2(\theta'[s])^2\psi_{w_j}[s]\psi_{w_k}[s]\dot{q}_{w_j}[t]\dot{q}_{w_k}[t]\}\, dx_3\, dy_3\, dz_3 \qquad (3.79)$$

From the kinetic energy expression shown in eq. (3.79) we can formulate the mass matrix as follows

1. Flat-wise only

$$\mathrm{m}_{\mathrm{jk}}^{\mathrm{uu}} = \frac{1}{2}\int_{0}^{\mathrm{S}} \{\mathrm{m}\psi_{\mathrm{u_j}}[\mathrm{s}]\psi_{\mathrm{u_k}}[\mathrm{s}] + \mathrm{I}_{\mathrm{my_3}}\psi_{\mathrm{u_j}}{}'[\mathrm{s}]\psi_{\mathrm{u_k}}{}'[\mathrm{s}]\}\,\mathrm{ds} \qquad (3.80)$$

2. Edge-wise only

$$\mathrm{m}_{\mathrm{jk}}^{\mathrm{vv}} = \frac{1}{2}\int_{0}^{\mathrm{S}} \{\mathrm{m}\psi_{\mathrm{v_j}}[\mathrm{s}]\psi_{\mathrm{v_k}}[\mathrm{s}] + \mathrm{I}_{\mathrm{mx_3}}\psi_{\mathrm{v_j}}{}'[\mathrm{s}]\psi_{\mathrm{v_k}}{}'[\mathrm{s}]\}\,\mathrm{ds} \qquad (3.81)$$

3. Extension only

$$m_{jk}^{ww} = \frac{1}{2}\int_0^S \{m\psi_{w_j}[s]\psi_{w_k}[s] + I_{my_3}(\theta'[s])^2\psi_{w_j}[s]\psi_{w_k}[s]\}\,ds \quad (3.82)$$

4. Torsion only

$$m_{jk}^{\phi\phi} = \frac{1}{2}(I_{mx_3} + I_{my_3})\int_0^S \{\psi_{\phi_j}[s]\psi_{\phi_k}[s]\}\,ds \quad (3.83)$$

5. Flat wise- edge wise

$$m_{jk}^{uv} = 0 \quad (3.84)$$

6. Flat wise-extension

$$m_{jk}^{uw} = -I_{my_3}\int_0^S \{\theta'[s]\psi_{u_j}'[s]\psi_{w_k}[s]\}\,ds \quad (3.85)$$

7. Flat wise-torsion

$$m_{jk}^{u\phi} = -me\int_0^S \{\psi_{u_j}[s]\psi_{\phi_k}[s]\}\,ds \quad (3.86)$$

8. Edge wise-extension

$$m_{jk}^{vw} = -me\int_0^S \{\psi_{v_j}'[s]\psi_{w_k}[s]\}\,ds \quad (3.87)$$

9. Edge wise-torsion

$$m_{jk}^{v\phi} = 0 \quad (3.88)$$

10. Extension-torsion

$$m_{jk}^{w\phi} = 0 \quad (3.89)$$

Note that the mass matrix of the blade is symmetric so we have

$$m_{jk}^{uv} = m_{jk}^{vu}$$

$$m_{jk}^{uw} = m_{jk}^{wu}$$

$$m_{jk}^{u\phi} = m_{jk}^{\phi u}$$

$$m_{jk}^{vw} = m_{jk}^{wv} \qquad (3.90)$$

$$m_{jk}^{v\phi} = m_{jk}^{\phi v}$$

$$m_{jk}^{w\phi} = m_{jk}^{\phi w}$$

3.4.3 Meridian angle (θ)

In the mass and stiffness expressions derived in section 3.4.2 we can see the parameter θ and its derivatives with respect to z_3 or s. This θ is known as the meridian angle and is defined as the angle between the tangent to the blade at any point in the elastic axis and the vertical axis at this point as shown in figure 2.17. For the simplified Sandia shape the meridian angle can be calculated as:

$$\theta = \frac{S_c}{R_c}$$

where

S_c**:** is the length of the circular segment of Sandia simplified shape blade

R_c: is the radius of the circular segment of Sandia simplified shape blade

$$\theta' = \frac{d\theta}{ds} = \frac{1}{R_c}$$

$$\theta'' = \frac{d^2\theta}{ds} = 0$$

3.5 Numerical calculation of modal frequencies of 17 m diameter Sandia simplified blade shape

In this section the analytical model developed in sections 3.2, 3.3, 3.4, was tested by using the derived modal mass and stiffness matrices expressions to calculate the first ten modal frequencies for 17 m diameter stationary simplified Sandia blade and comparing it with the finite element modal analysis results.

3.5.1 17 m diameter simplified Sandia blade cross section properties

The blade cross section geometric and mass related parameters are calculated here for the NASA 0015 blade cross section shown in figure 2.2 as follows

$A = 0.98 * 10^{-2}\ m^2$

$I_{y_3y_3} = 0.859 * 10^{-5} m^4$

$Ae_A = -0.001434 m^3$

$I_{x_3x_3} = 2.814 * 10^{-4} m^4$

$P_1 = 2.897 * 10^{-9}\ m^6$

$P_2 = -6.8499 * 10^{-7} m^5$

$P_3 = 1.816 * 10^{-7}\ m^6$

$\lambda_1 = 4.730040744862704$

$\lambda_2 = 7.853204624095838$

$\lambda_3 = 10.995607838001671$

$\lambda_4 = 14.137165491257464$

$\lambda_5 = 17.27875965739948$

$\lambda_6 = 20.42035224562606$

$\lambda_7 = 23.561944902040455$

$E = 68.95 * 10^9 N/m^2$

$G = 25.86 * 10^9 N/m^2$

$m = 30.5 kg/m$

$me = -3.97 Kg$

$I_{mx_3} = 1.5\ kg.m$

$I_{my_3} = 0.0247\ kg.m$

Blade length S = 30.47m

Meridian angle θ= 46.36^{o} for straight segments

Meridian angle θ is variable for circular segments

θ'= θ''=0 for straight segments

θ'= 0.096 rad/m for circular segment

θ''=0 for circular segment

3.5.2 Numerical values for first ten modal frequencies

Substituting the cross section parameters values calculated in section 3.5.1 in addition to the blade length (S) and the meridian angle (θ) in the modal mass and stiffness sub-matrices equations and varying the summation parameters values (j and k) we got the best convergence at (j=k=7). When j=k=7, and all flat wise, edge wise, torsion, and extension modes included, modal mass and stiffness gives the first 28 modal frequencies as shown in table 3.1

Table 3.1 modal frequencies for 17 m diameter Sandia stationary blade (coupling between all modes considered

modal frequencies (1 to 14)	**modal frequencies (15 to 28)**
1.5564	83.2925
3.00157	93.1968
4.32495	124.232
8.4747	134.915
10.254	162.029
11.7791	180.423

Table 3.1 (cont'd)	
13.9191	218.931
15.5556	236.816
20.0909	263.703
23.5478	310.944
27.9191	327.779
49.2278	388.544
50.7068 i	462.103
55.4277	540.848

From table 3.1 we can see that the lowest seven modal frequencies are of a similar order of magnitude as the first seven modal frequencies calculated using the FE model in chapter 2 with around 70% so the error here is around 30% which is not acceptable. Also the modal frequency number 13 in red color is complex and this is not allowed because the mass and stiffness matrices are supposed to be positive definite, and symmetric. The K matrix contains some asymmetric terms. The terms are small compared to other terms in the K matrix. They may be due to numerical errors, but in a continuing investigation we are examining this further.

Because we followed a good derivation procedure to get expressions for kinetic and potential energies and we checked that these equations are physically and dimensionally correct, the sources of results inconsistency with our finite element model and Sandia finite element model results may be because of some programming errors in the Mathematica code for calculating modal frequencies and mode shapes, or because of unsuitable selection

of assumed modal functions. One of our future plans for this work is to replace these assumed modal functions, which contain hyperbolic terms, with polynomial ones which are better conditioned, and then seek better convergence for our analytical model.

4 Chapter 4

4.1 Conclusion and comments

As a result of this research work:

1. FEM model for troposkein-shaped Darrieus wind turbine blade free vibration has been built for both ideal and simplified shapes. The blade vibration under flat-wise, edge-wise, extensional, and torsional deformations was studied and the lowest ten modes have been characterized for stationary and rotating blade conditions.
2. Energy equations for a troposkein blade under the same loading conditions mentioned above were derived. We have made initial progress on the low-order model of the curved blade. We have followed an analysis from a 1979 NASA paper by K and K, and extended it by performing an assumed-mode discretization. However, the predicted frequencies from the reduced-order model are not yet matching well. Possible problems are listed below. Nonetheless, the work sets up the next student to review and validate the analysis process, and then apply low-order modeling.
3. Possible problems in the low-order model are as follows
    a) The use of clamped-clamped assumed modes. These modal functions involve hyperbolic functions, which have extreme values when the arguments become large. (However, the first mode won't have this issue, and it is not producing satisfactory estimations)
    b) The use of clamped-clamped boundary conditions in the beam model may not accurately represent the connections in the finite element analysis (However, this should be a stiffening assumption, and lead to over-predicted frequencies)

c) The strain formulation followed in KK 1979 involves several rotating, deformation dependent, coordinate transformations, and the algebra should be validated once again. This is in progress.

4.2 Contribution

Because of the shortage in studying Darrieus wind turbine blade vibration, this work has provided an initial contribution to research literature toward developing the study of Darrieus wind turbine blade vibration.

The model developed here can be used for characterization of Darrieus wind turbine blade modal vibration analytically and these results can be compared to the numerical (FEM) results for validation.

4.3 Future work

Based on this work some follow-up studies will be useful. Some of the future work includes.

- More development in the analytical model to correct its erroneous results, which makes it valid for analytical characterization of Darrieus wind turbine blade modal vibration
- Studying Darrieus wind turbine blade forced vibration under aerodynamic loadings
- Modeling Darrieus wind turbine blade vibration considering higher order terms using nonlinear techniques (for example perturbation methods)

APPENDIX

Table.1 blade airfoil coordinates

x	x/c	camber line(Yc)	yt	θ	Xu	Yu	XL	YL
0	0	0	0	0	0	0	0	0
1	0.016393	0	1.640381	0	1	1.640381364	1	-1.640381364
2	0.032787	0	2.253687	0	2	2.25368702	2	-2.25368702
3	0.04918	0	2.691405	0	3	2.691405028	3	-2.691405028
4	0.065574	0	3.034709	0	4	3.034709024	4	-3.034709024
5	0.081967	0	3.315231	0	5	3.3152312	5	-3.3152312
6	0.098361	0	3.54934	0	6	3.549340183	6	-3.549340183
7	0.114754	0	3.746877	0	7	3.746876512	7	-3.746876512
8	0.131148	0	3.914348	0	8	3.914348168	8	-3.914348168
9	0.147541	0	4.056357	0	9	4.056356584	9	-4.056356584
10	0.163934	0	4.176321	0	10	4.176321059	10	-4.176321059
11	0.180328	0	4.276882	0	11	4.276882334	11	-4.276882334
12	0.196721	0	4.360144	0	12	4.360143598	12	-4.360143598
13	0.213115	0	4.427822	0	13	4.427822451	13	-4.427822451
14	0.229508	0	4.481351	0	14	4.481351006	14	-4.481351006
15	0.245902	0	4.521944	0	15	4.52194425	15	-4.52194425
16	0.262295	0	4.550648	0	16	4.55064816	16	-4.55064816
17	0.278689	0	4.568374	0	17	4.568374455	17	-4.568374455
18	0.295082	0	4.575926	0	18	4.575926263	18	-4.575926263
19	0.311475	0	4.574017	0	19	4.574017431	19	-4.574017431
20	0.327869	0	4.563287	0	20	4.563287327	20	-4.563287327
21	0.344262	0	4.544312	0	21	4.544312334	21	-4.544312334
22	0.360656	0	4.517615	0	22	4.517614914	22	-4.517614914
23	0.377049	0	4.483671	0	23	4.483670829	23	-4.483670829
24	0.393443	0	4.442915	0	24	4.442914969	24	-4.442914969
25	0.409836	0	4.395746	0	25	4.395746095	25	-4.395746095
26	0.42623	0	4.342531	0	26	4.342530731	26	-4.342530731
27	0.442623	0	4.283606	0	27	4.283606395	27	-4.283606395
28	0.459016	0	4.219284	0	28	4.219284293	28	-4.219284293
29	0.47541	0	4.149852	0	29	4.149851581	29	-4.149851581
30	0.491803	0	4.075573	0	30	4.075573284	30	-4.075573284
31	0.508197	0	3.996694	0	31	3.996693923	31	-3.996693923
32	0.52459	0	3.913439	0	32	3.913438914	32	-3.913438914
33	0.540984	0	3.826016	0	33	3.826015767	33	-3.826015767
34	0.557377	0	3.734615	0	34	3.734615124	34	-3.734615124
35	0.57377	0	3.639412	0	35	3.639411661	35	-3.639411661
36	0.590164	0	3.540565	0	36	3.540564874	36	-3.540564874
37	0.606557	0	3.43822	0	37	3.438219769	37	-3.438219769
38	0.622951	0	3.332507	0	38	3.332507465	38	-3.332507465

Table.1 (cont'd)

39	0.639344	0	3.223546	0	39	3.223545733	39	-3.223545733
40	0.655738	0	3.111439	0	40	3.111439463	40	-3.111439463
41	0.672131	0	2.996281	0	41	2.996281088	41	-2.996281088
42	0.688525	0	2.878151	0	42	2.878150957	42	-2.878150957
43	0.704918	0	2.757118	0	43	2.75711767	43	-2.75711767
44	0.721311	0	2.633238	0	44	2.633238376	44	-2.633238376
45	0.737705	0	2.506559	0	45	2.506559046	45	-2.506559046
46	0.754098	0	2.377115	0	46	2.377114708	46	-2.377114708
47	0.770492	0	2.24493	0	47	2.244929673	47	-2.244929673
48	0.786885	0	2.110018	0	48	2.11001773	48	-2.11001773
49	0.803279	0	1.972382	0	49	1.972382324	49	-1.972382324
50	0.819672	0	1.832017	0	50	1.832016723	50	-1.832016723
51	0.836066	0	1.688904	0	51	1.688904161	51	-1.688904161
52	0.852459	0	1.543018	0	52	1.543017978	52	-1.543017978
53	0.868852	0	1.394322	0	53	1.394321742	53	-1.394321742
54	0.885246	0	1.242769	0	54	1.242769361	54	-1.242769361
55	0.901639	0	1.088305	0	55	1.08830519	55	-1.08830519
56	0.918033	0	0.930864	0	56	0.930864123	56	-0.930864123
57	0.934426	0	0.770372	0	57	0.770371683	57	-0.770371683
58	0.95082	0	0.606744	0	58	0.606744102	58	-0.606744102
59	0.967213	0	0.439888	0	59	0.439888396	59	-0.439888396
60	0.983607	0	0.269702	0	60	0.269702434	60	-0.269702434
61	1	0	0.096075	0	61	0.096075	61	-0.096075

BIBLIOGRAPHY

BIBLIOGRAPHY

[1] Figure 1.1 taken from https://en.wikipedia.org/wiki/Wind_power web page.

[2] Wind Turbines: Fundamentals, Technologies, Application, Economics, by Erich Hau, 2nd edition, 2006, Springer, Germany.

[3] http://www.reuk.co.uk/wordpress/wind/savonius-wind-turbines.

[4] https://upload.wikimedia.org/wikipedia/commons/9/9e/Darrieus.jpg.

[5] G. J. M. Darrieus, "Turbine Having its Rotating Shaft Transverse to the Flow of the Current, "United States Patent No. 1, 835, 018, December 8, 1931.

[6] Wind Turbine Design: With Emphasis on Darrieus Concept, By Ion Paraschivoiu, Presses internationals Polytechnique, 2002, Canada.

[7] Blade shape for troposkien type of vertical-axis wind turbine B. F. Blackwell, G. E. Reis Sandia National Laboratories; Albuquerque, NM 87185, April 1974.

[8] P. South and R. S. Rangi, Preliminary Tests of a High Speed - Vertical Axis Windmill Model, National Research Council of Canada, LTR-LA-74, March 1971.

[9] P, South and R. S. Rangi, "The Performance and Economics of the VerticalAxis Wind Turbine Developed at the National Research Council, Ottawa, Canada, " Agricultural Engineer, February 1974, pp. 14-16. (See also American Society of Agricultural Engineers, Paper No. PNW 73-303).

[10] "Aeroelastic equations of motion of Darrieus vertical axis wind turbine blade" by Krishna Rao V. Kaza, and Raymond G. Kvaternik- DOE/NA SA11028-79125/NASA TM-79295, December 1979.

[11] Alcoa Laboratories. Design and fabrication of a low cost Darrieus vertical axis wind turbine system, phase 1. Technical Report, ALO-4272:1-236, June 22 1979.

[12] Bennie F. Blackwell, Robert E. Sheldahl , "Wind unnel performance data for the Darrieus wind turnine with NACA 0012 blades" Aerothermodynamics Division, 1333 Louis V. Feltz Mechanical Design Division, 1324 Sandia Laboratories Albuquerque, NM 87115, May 1976.

[13] Owens, B.C., and Griffith, D.T., "Aeroelastic Stability Investigations of Large-scale Vertical Axis Wind Turbines," Journal of Physics Conference Series, Science of Making Torque from Wind Conference, June 18–20, 2014, Lyngby, Denmark.

[14] Owens, B., Hurtado, J., Barone, M., and Paquette, J., "An Energy Preserving Time Integration Method for Gyric Systems: Development of the Offshore Wind Energy Simulation Toolkit" *Proceedings of the European Wind Energy Association Conference & Exhibition.* Vienna, Austria, 2013.

[15] Owens, B.C., Hurtado, J.E., Paquette, J., Griffith, D.T., and Barone, M., "Aeroelastic Modeling of Large Offshore Vertical-axis Wind Turbines: Development of the Offshore Wind Energy Simulation Toolkit," *54thAIAA/ASME/ASCE/AHS/ASC Structures, Structural Dynamics, and Materials Conference*, April 8–11, 2013, Boston, MA, USA, AIAA-2013-1552.

[16] Owens, B.C., Griffith, D.T., and Hurtado, J.E., "Modal Dynamics and Stability of Large Multi-megawatt Deepwater Offshore Vertical-axis Wind Turbines: Initial Support Structure and Rotor Design Impact Studies," 32nd ASME Wind Energy Symposium, National Harbor, MD, USA, January 2014.

[17] Simao Ferreira, C., Schmidt Paulson, U., Griffith, D. T., Borg, M., eds., 2016, Scientific and Technical Challenges in Offshore Vertical Axis Wind Turbines, Euromech Colloquium 583, September 7-9, Delft, the Netherlands.

[18] Equation 2.2 taken from https://en.wikipedia.org/wiki/NACA_airfoil.

[19] www.sharcnet.ca/Software/Ansys/17.0/en-us/help/ans_elem/Hlp_E_SOLID187.

[20] G. Thomas Mase and George E. Mase, "Continuum Mechanics for Engineers", 1999 by CRC Press LLC, New York.

[21] Singiresu S. Rao, "Vibration of Continuous Systems", 2007 by John Wiley & Sons, Inc, New Jersey.